The barley mutant *multiflorus2.b* reveals quantitative genetic variation for new spikelet architecture

Ravi Koppolu[1‡*], Guojing Jiang[1‡], Sara G Milner[1], Quddoos H Muqaddasi[1,3], Twan Rutten[1], Martin Mascher[1], Thorsten Schnurbusch[1,2*]

[1]Leibniz Institute of Plant Genetics and Crop Plant Research (IPK), Correns Strasse 3, OT Gatersleben, 06466 Seeland, Germany.

[2]Institute of Agricultural and Nutritional Sciences, Faculty of Natural Sciences III, Martin Luther University Halle-Wittenberg, 06120 Halle, Germany

[3] Current address: BASF Agricultural Solutions GmbH, Am Schwabeplan 8, OT Gatersleben, 06466 Seeland, Germany

‡Ravi Koppolu and Guojing Jiang contributed equally

*Corresponding authors:

Ravi Koppolu (koppolu@ipk-gatersleben.de);

Thorsten Schnurbusch (schnurbusch@ipk-gatersleben.de)

ORCIDS

R.K. 0000-0001-8566-9501

G.J. 0000-0002-4335-1527

S.G.M.

Q.H.M. 0000-0001-5961-7273

T.R. 0000-0001-5891-6503

MM. 0000-0001-6373-6013

T.S. 0000-0002-5267-0677

Abstract

Understanding the genetic basis of yield forming factors is of utmost importance especially in the wake of stagnation of further yield gains in small grain cereals. One such yield forming factor in these cereals is the number of grain-bearing florets produced per spikelet. Generally, the spikelet axis (rachilla) of determinate barley (*Hordeum vulgare* L.) spikelets degenerates after producing one floret. In contrast, the rachilla of indeterminate wheat (*Triticum ssp.*) spikelets elongates to produce up to 12 florets. In our study, we characterized the barley spikelet determinacy mutant *multiflorus2.b* (*mul2.b*) that produced up to three fertile florets on elongated rachilla of lateral spikelets. Apart from the lateral spikelet indeterminacy (LS-IN), we also characterized the supernumerary spikelet phenotype in the central spikelets (CS-SS) of *mul2.b.* Through our phenotypic and genetic analyses, we identified two major QTLs on chromosomes 2H and 6H, along with two minor QTLs on 3H for the LS-IN phenotype. For, the CS-SS phenotype we identified a major QTL on 6H, along with one minor QTL on 5H. Notably, the 6H QTLs for CS-SS and LS-IN phenotypes co-located with each other, potentially indicating that a single genetic factor might regulate both phenotypes. Thus, our in-depth phenotyping combined with genetic analyses revealed the quantitative nature of the LS-IN and CS-SS phenotypes in *mul2.b*, paving way for cloning the genes underlying these QTLs in the future.

63 **Introduction**

64 Grass inflorescences are constituted by the ordered arrangement of spikelets (specialized
65 flower-bearing structures) either on the branches differentiated from the inflorescence
66 axis (rachis) or directly on the inflorescence axis. The *Triticeae* grasses display
67 characteristic spike-shaped inflorescences with sessile spikelets attached to the
68 inflorescence axis in a distichous phyllotaxis (Bonnett 1935, 1936; Kellogg et al. 2013).
69 Among *Triticeae*, wheat (*Triticum spp.*) and barley (*Hordeum spp.*) represent the most
70 economically important temperate cereal species (Schnurbusch 2019). Based on the
71 architectural differences at the spikelet and spike levels, wheat and barley inflorescences
72 can be classified into (i) determinate or (ii) indeterminate spikes (Bonnett 1966). In the
73 determinate spikes of wheat, the inflorescence apex culminates with a terminal spikelet
74 thus producing a fixed number of spikelets per inflorescence. However, the spikelets in
75 the wheat spike are indeterminate with multiple flowers (florets; up to 12), each
76 produced at the articulation junction of the spikelet axis called rachilla (**Fig. 1E)**. In
77 contrast, the inflorescence apex of barley remains indeterminate (no terminal spikelet)
78 and the rachilla ceases to grow upon initiation of the first floret and remains as a
79 suppressed structure rendering determinacy to the spikelet (**Fig. 1B**). Thus the spikelet
80 determinacy or indeterminacy is dependent upon the extent of rachilla suppression or
81 elongation.

82

83 The genetic control of determinate spikelet fate was studied in rice, wheat, and maize. In
84 these three species, orthologous APETALA 2 (AP2) transcription factors, such as maize
85 INDETERMINATE SPIKELET1 (IDS1)/TASSELSEED 6 (Chuck et al. 2008; Chuck et al.
86 2007; Chuck et al. 1998), rice IDS1 (Lee and An 2012), and wheat Q (*AP2L5*) (Debernardi
87 et al. 2017; Greenwood et al. 2017; Simons et al. 2006), were shown to negatively control
88 floret number per spikelet by inhibiting rachilla elongation. The paralog of maize *IDS1*,
89 sister of *IDS1* (*SIDS1*), and rice *SUPERNUMERARY BRACT* also regulate floret number per
90 spikelet by inhibiting rachilla elongation (Chuck et al. 2008; Lee and An 2012; Lee et al.
91 2007). Interestingly, the corresponding barley ortholog of *IDS1*, *HvAP2L-H5*, was shown
92 to promote the indeterminate nature of the inflorescence apex and also spikelet
93 determinacy probably by regulating rachilla elongation (Zhong et al. 2021). Apart from
94 the *Q* gene in wheat, the *GRAIN NUMBER INCREASE 1* (*GNI1*) is shown to inhibit rachilla
95 development and growth and thereby regulates floret number per spikelet (Sakuma et al.
96 2019; Sakuma and Schnurbusch 2020). The *sham ramification 1* (*shr1*) and *shr2* mutants

in tetraploid wheat show an elongated rachilla. The genes underlying these loci are not known yet (Amagai et al. 2014).

In rice, several other genes were characterized that potentially regulate spikelet determinacy. These include *LEAFY HULL STERILE 1* (*OsMADS1* (Jeon et al. 2000)), *MOSAIC FLORAL ORGANS* 1 (*AGAMOUS LIKE 6* (Ohmori et al. 2009)), and *MULTIFLORETSPIKELET1* (*AP2/ERF*; (Ren et al. 2013)). Mutations in these genes promote rachilla elongation and extra floret formation rendering the indeterminate spikelet fate. Apart from these, rice genes such as *DOUBLE FLORET1/EXTRA GLUME 1*, *FLORAL ORGAN NUMBER 4*, *TONGARI-BOUSHI 1*, and *LATERAL FLORET 1* are also shown to regulate the floret number/spikelet probably through suppression of rachilla elongation (Ren et al. 2019; Ren et al. 2018; Tanaka et al. 2012; Zhang et al. 2017). The results from these studies provided us with a lead that the spikelet determinacy is a plastic trait modulated by the genetic makeup of respective grass species and that the extent of rachilla elongation or suppression potentially defines the floret number per spikelet.

Within Triticeae, barley shows a distinctive spike architecture, imparted by the distichously arranged triple-spikelet units along the rachis. Each spikelet triplet is constituted by one central (CS) and two lateral spikelets (LS), the two- and six-rowed barley row-type classes are defined based on the fertility status at the LSs. In two-rowed barley, the CSs are fertile, produce grains, while LSs remain sterile. Whereas in six-rowed, both CSs and LSs are fertile and bear grains. The fertility status of lateral spikelets is majorly regulated by the *SIX-ROWED SPIKE 1* (*VRS1,* class I HD-ZIP; (Komatsuda et al. 2007)), along with other regulators/modifier genes (Bull et al. 2017; Koppolu et al. 2013; Ramsay et al. 2011; van Esse et al. 2017; Youssef et al. 2017). Thus, the archetypical barley spike possesses one CS positioned on the spike axis with an acute angle, flanked by two LSs positioned slightly away from the spike axis. In wheat, a single spikelet per rachis node is generated with an acute angle to the rachis similar to barley CS. In both wheat and barley, spike mutants that deviate from such a canonical arrangement of spikelets exist that have the potential to generate more spikelets and grains. In barley, a class of mutants called *extrafloret* (*flo*; *flo-a, -b, and -c*) develop either a complete extra or supernumerary spikelet or rudimentary floral bracts (the locus name *extrafloret* is a misnomer) at the base of typical CS on the abaxial side of the same rachis node (Druka et al. 2011; Franckowiak 1995). The causal genes underlying these loci are not known. A similar

131 supernumerary spikelet (SS) phenotype is also evident in mutants of barley
132 *COMPOSITUM1* (Poursarebani et al. 2020), *COMPOSITUM2* (Poursarebani et al. 2015))
133 and *VRS4* (Koppolu et al. 2013). The wheat ortholog of barley *COM2* was also shown to
134 regulate SS formation in hexaploid (Dobrovolskaya et al. 2015) and tetraploid branched
135 miracle wheat (*TtBH*^{t}; (Sakuma and Schnurbusch 2020; Wolde et al. 2019). Away from
136 these genes, the SS phenotype in wheat is also conditioned by the photoperiod-dependent
137 floral induction gene, *PHOTOPERIOD 1* (*PPD1*), and the axillary meristem growth
138 regulator *TEOSINTE BRANCHED 1* (*TB1*). Both *PPD1* and *TB1* regulate SS formation by
139 regulating *FLOWERING LOCUS T1* (*FT1*) that induces a cascade of floral meristem identity
140 genes important for floral induction (Boden et al. 2015; Dixon et al. 2018).
141
142 In this study, we investigated the inheritance of spikelet determinacy (floret number per
143 spikelet) and supernumerary spikelet phenotypes in a barley *X*-ray induced mutant
144 "*multiflorus2.b*" (progenitor – Montcalm). This barley *mul2.b* mutant produces non-
145 canonically a multi-floreted, indeterminate spikelet phenotype on its elongated rachilla, a
146 feature reminiscent of wheat spikelets. Moreover, from our in-depth mutant phenotyping
147 and allelism analyses we show that *mul2.b* also induces the supernumerary spikelet
148 phenotype. Based on our analyses using exome capture-based bulked-segregant analysis,
149 genetic and QTL mapping studies, we reveal that the multi-floreted and supernumerary
150 spikelet phenotypes have a quantitative inheritance pattern.
151
152 **Materials and Methods**
153 ***Plant material and growth conditions***
154 All experiments reported in this study were conducted at the Leibniz Institute of Plant
155 Genetics and Crop Plant Research, Gatersleben, Germany. The genotypes cv. Montcalm,
156 cv. Morex, *multiflorus2.b* (*mul2.b;* GSHO 1394) – a betatron induced *X*-ray mutant of
157 Montcalm, and Bowman Near Isogenic line mutant *extra floret.a* – BM-NIL(*flo.a*), were
158 used for various analyses conducted in this study. The majority of experiments in this
159 study were conducted under greenhouse conditions at the IPK in the period between
160 2014 and 2020. For greenhouse experiments, initially, barley grains were germinated in
161 96 well planting trays and grown at 16h/8h (light/dark; photoperiod), and, 20° C/16° C
162 (light/dark; temperature) for two weeks. After collecting leaf material for DNA extraction,
163 the plants were vernalized at 4° C for four weeks and then acclimatized at 15° C in the
164 greenhouse for a week. Later the plants were potted into 14 cm (Ø) pots and grown at

165 16h/8h (light/dark; photoperiod), and, 20° C/16° C (light/dark; temperature) until
166 maturity. Standard practices for irrigation, fertilization, and control of pests and diseases
167 were followed. The genotypes Montcalm and *mul2.b* were evaluated under field
168 conditions in 2015 and 2016 at IPK for the grain morphometry parameters. Each
169 genotype was grown in three independent plots measuring 1 × 1.5 m^2, with a sowing
170 density of 300 grains/m^2. Each plot had six rows with 20 cm spacing between rows.
171

172 ***Mapping populations and phenotyping***

173 For mapping of the traits lateral spikelet indeterminacy (LS-IN) and central spikelet
174 supernumerary spikelet (CS-SS) phenotypes, the mutant parent *mul2.b* was crossed with
175 Morex and Montcalm to generate two independent mapping populations, Morex × *mul2.b*
176 and *mul2.b* × Montcalm. The F_1 hybrids were selfed and the resulting F_2 and $F_{2:3}$
177 populations were used for phenotypic and genotypic analyses. To test the allelism
178 between *mul2.b* and BM-NIL(*flo.a*), reciprocal crosses were made between the two
179 mutants, and the CS-SS phenotype were analyzed at F_1 and F_2 generations.

180 The Morex × *mul2.b* (POP 2014-1; 163 F_{2s}) and *mul2.b* × Montcalm (POP 2014-2; 130 F_{2s})
181 populations were initially phenotyped in 2014 under greenhouse conditions. The LS-IN
182 phenotype was scored as strong and moderate to weak classes based on visual
183 observation of rachilla elongation or extra floret phenotype in all spikes of each F_2 line
184 after grain filling. F_2 plants with strong phenotype showed approximately 75% of spikes
185 with a second floret that either produced a grain or remained empty. Whereas the F_2 lines
186 that showed elongated rachilla or improperly formed second floret were scored into weak
187 to moderate phenotype class. The CS-SS phenotype in central spikelets was quantified by
188 counting the number of occurrences of extra spikelets or rudimentary bract-like
189 structures on all spikes of each F_2 line.

190 In 2015, we phenotyped Morex × *mul2.b* population again under greenhouse conditions
191 (136 F_{2s}; POP 2015) by quantifying both LS-IN and CS-SS phenotypes. For quantification,
192 of LS-IN phenotype we classified the phenotype into *mul2.b* class-*I, -II, -III,* and -*IV* based
193 on the additional floret or rachilla elongation phenotype (please see results section for
194 the description of each phenotypic class). The number of instances of *mul2.b-I, -II, -III,* and
195 -*IV* phenotypes were recorded for all lateral spikelet positions on spike-bearing tillers of
196 each F_2 line. Similarly, the number of instances of supernumerary spikelets born from the
197 central spikelet region was counted.

198 In 2016, a larger F_2 population of Morex × *mul2.b* was further phenotyped under
199 greenhouse conditions (179 F_{2s}; POP 2016) for the LS-IN and CS-SS phenotypes. The
200 phenotype quantification data from POP 2016 was used for whole-genome QTL mapping.

201 For scoring the CS-SS trait in F_2 lines of BM-NIL(*flo.a*) × *mul2.b*, the phenotype was
202 classified into six classes. These include WT (no phenotype), very weak (one spike with
203 CS-SS phenotype out of all spikes/plant), weak (~10-15% of spikes with CS-SS
204 phenotype), Moderate (~25% of spikes with CS-SS phenotype), strong (~50% of spikes
205 with CS-SS phenotype), and very strong (~75-100% of spikes with CS-SS phenotype)
206

207 ***Grain morphometry analysis of Montcalm and mul2.b***

208 To evaluate the grain morphometry parameters of Montcalm and *mul2.b*, the spikes from
209 the field (2015 and 2016) and greenhouse (2020) grown plants were hand-harvested and
210 threshed. The representative grain samples from each genotype (3 to 4 grain
211 samples/plot/genotype) were analyzed for the thousand-grain weight (TGW), grain area
212 (mm^2), grain width (mm), and grain length (mm) using a digital seed analyzer/counter
213 Marvin (GTA Sensorik GmbH, Neubrandenburg, Germany). From the greenhouse
214 experiment (2020), the grain morphometry parameters were collected for central and
215 lateral spikelet grains independently. For this analysis, central and lateral spikelet grains
216 of twelve independent plants from each genotype were used. Apart from these, traits such
217 as plant height, total, productive, unproductive tillers were scored from the greenhouse
218 experiment (2020).
219

220 ***Phenotyping of Montcalm and mul2.b immature spikes***

221 Immature spikes of Montcalm and *mul2.b* genotypes were phenotyped from Waddington
222 stage W2.0 (double ridge) to W6.0 (Waddington et al. 1983) to follow rachilla
223 development in lateral spikelets. The spike meristems from respective genotypes were
224 hand dissected and staged under a stereomicroscope (Zeiss Stemi 2000-C; Carl Zeiss™).
225 The maximum yield potential in Montcalm and *mul2.b* was counted on the main culm
226 spike approximately at W8.0 (number of rachis nodes per spike ∗ three spikelets per
227 node).
228

229 ***Scanning electron microscopy***

230 Scanning electron microscopy (SEM) was performed on immature spikes that are
231 approximately at W4.0, W4.5, W5.0, W5.5, and W6.0 from greenhouse-grown plants. SEM
232 was conducted following an established protocol at IPK (Lolas et al. 2010; Poursarebani
233 et al. 2020).
234
235 ***Exome sequencing - Morex × mul2.b – POP 2014-1***
236 For exome sequencing, the DNAs from 25 wild type and 27 mutant F_2 lines were bulked
237 from Morex × *mul2.b* population grown in 2014. The two DNA bulks were subjected to
238 exome capture and sequencing according to the previous protocol (Mascher et al. 2013).
239 Read mapping, allele frequency visualization, and read depth analysis of exome
240 sequencing data of mutant and wild-type bulks were done as described in Mascher et al.
241 (2014) using the BAC-based reference sequence of cv. Morex (Mascher et al. 2017).
242
243 ***Marker development, linkage, and QTL analysis on 2H and 6H chromosomes***
244 The LS-IN and CS-SS phenotype data from Morex × *mul2.b* – 2015 (POP 2015) was used
245 for marker and phenotype linkage analysis on 2H and 6H barley chromosomes. For
246 mapping, the polymorphic SNPs were selected based on exome capture SNPs from
247 chromosomes 2H and 6H where the allele frequency differences between mutant and wild
248 type bulks reached their high. On chromosome 2H, 11 SNPs were selected in the interval
249 33.70 – 87.70 cM (Morex POPSEQ positions). On 6H, seven SNPs were selected in the
250 interval 31.90 – 92.20 cM. The selected SNPs were converted to restriction enzyme-based
251 Cleaved Amplified Polymorphic Sequence (CAPS) markers (**Supplementary Table 1**)
252 using Neb cutter v2.0 (New England Biolabs Inc). Restriction digestion was performed
253 according to the manufacturer's protocols. The resulting DNA fragments were separated
254 on 2% agarose gels for genotyping. The genotypic and phenotypic data were subjected to
255 linkage and QTL analyses in Joinmap 4.1 and Genstat 19 respectively.
256
257 ***GBS library construction, sequencing, read alignment, and variant calling***
258 The total genomic DNA from the F_2 lines of Morex × *mul2.b* (POP 2016) was extracted as
259 described in Poursarebani et al. (2020). Genomic DNA was digested with *PstI* and *MspI*
260 restriction enzymes and processed for GBS library construction as described in Wendler
261 et al. (2014). Individually barcoded samples were pooled in equimolar concentrations and
262 single read sequenced on the Illumina HiSeq 2500 (1 × 107 cycles), using custom

263 sequencing primer (Wendler et al. 2014) as given in manufacturers protocol (Illumina
264 Inc).

265 GBS reads were trimmed using cutadapt (Martin 2011) and aligned to the reference
266 genome sequence of Morex (Mascher et al. 2017) with BWA-MEM v0.7.12a (Li 2013). The
267 alignment files were then converted to binary alignment map (BAM) format with
268 SAMtools (Li et al. 2009), sorted by reference position, and indexed with NovoSort
269 (Novocraft Technologies Sdn Bhd, Malaysia, http://www.novocraft.com/). Variants were
270 called using SAMtools/BCFtools v1.3 specifying the option '-DV' while running SAMtools
271 mpileup (Li 2011)), to obtain the per-sample number of non-reference reads. An AWK
272 script (available at https://bitbucket.org/ipk_dg_public/vcf_filtering) was used to filter
273 the Variant Call Format (VCF) output file and call genotypes based on the ratio between
274 the depth of the alternative allele and the total read depth (DV /DP). A minimum mapping
275 quality score of 40 was required. The SNP matrix was created applying the following
276 threshold: a minimum read depth of 2X per genotype and an overall maximum fraction of
277 missing calls of 80%. Only biallelic SNPs were considered. We filtered the data for SNPs
278 with ≤10% missing data points, two or more linked markers showing identical marker
279 scores across all F_2 lines (no recombination), and variants showing distorted marker
280 scores. The final variant set was composed of 605 markers and was used for the genetic
281 linkage mapping and QTL analyses.

282 ***Whole-genome linkage mapping with GBS markers***

283 The genetic linkage maps were constructed with data from 605 GBS markers. The
284 markers were initially grouped according to the SNP physical position assignment based
285 on Morex reference. The markers from each group were then ordered using the maximum
286 likelihood mapping algorithm and default linkage parameters in Joinmap 4.1. The
287 recombination frequencies between markers were converted to map distances by the
288 Kosambi mapping function.

289 ***Phenotypic data analyses - Morex × mul2.b – POP 2016***

290 The phenotypic data for LS-IN and CS-SS traits were collected from up to 12 tillers. To
291 calculate the individual variance components of the genotype, tillers, and the residuals,
292 the following linear mixed-effect model was used by assuming all effects except the
293 intercept as random:

294 $$y_{ij} = \mu + g_i + t_j + \varepsilon_{ij} \quad (1)$$

where, y_{ij} is the phenotypic value of the ith genotype in the jth tiller, μ is the common intercept term, g_i is the effect of the ith genotype, t_j is the effect of the jth tiller, and ε_{ij} is the corresponding residual term as $\varepsilon \sim N(0, I\sigma_\varepsilon^2)$ with I and σ_ε^2 being the identity matrix and residual variance, respectively. The repeatability (H^2) among the tillers was accordingly calculated as:

$$H^2 = \frac{\sigma_g^2}{\sigma_g^2 + \left(\frac{\sigma^2_{\sigma_\varepsilon^2}}{nT}\right)} \quad (2)$$

Where, σ_g^2 and σ_ε^2 denote the variance components of the genotype and residuals, respectively; nT represent the number of tillers. The best linear unbiased estimations (BLUEs) across tillers for a given genotype were calculated by assuming the intercept and genotype effects as fixed in eq. 1. It should be noted that we evaluated the traits in F_2 populations; and therefore, we studied single plants by necessity. The calculations mentioned above were performed to (i) observe if there exists large and significant ($P < 0.001$) variance for spike bearing tillers, and (2) normalize the phenotypic value of the investigated traits per spike since it gives a more meaningful view of the studied traits. The BLUEs are plotted in the form of histograms. To observe the genetic nature of the investigated traits, the Shapiro-Wilk test was performed to monitor if the data were normally distributed at $P < 0.05$. Moreover, to observe the genetic relationship among the investigated traits, Pearson's product-moment correlation was calculated based on the BLUEs as:

$$r = \frac{\sum_{i=1}^{n}(x_i - \bar{x})(y_i - \bar{y})}{\sqrt{\sum_{i=1}^{n}(x_i - \bar{x})^2}\sqrt{\sum_{i=1}^{n}(y_i - \bar{y})^2}} \quad (3)$$

Where x and y denote the BLUEs of the studied traits. Unless stated otherwise, all calculations were performed in software R (R core team) using package lme4 (Bates et al. 2015).

Whole-genome QTL mapping in Morex × mul2.b – POP 2016

The BLUEs estimated from LS-IN (*mul2.b-I, -II, III*, and *-IV*) and CS-SS phenotypes along with 605 GBS marker data were used for QTL mapping in Genstat 19. Initially, simple interval mapping (SIM) was conducted with single environment, single trait linkage analysis. A step size of 5cM, genome-wide significance level (alpha) of 0.05, minimum co-

324 factor proximity of 50 cM were used for QTL detection. The minimum separation distance
325 for two consecutive QTLs was set at 30 cM. The co-factors identified from SIM were used
326 for QTL analysis by composite interval mapping (CIM). This process was repeated until
327 no new QTLs were detected. The final QTL model was selected based on background
328 selection (significance 0.05) on the selected co-factors. The QTL boundaries (lower and
329 upper), additive, dominance effects, phenotypic variation explained by the QTL were
330 defined by using the final QTL model. The procedure is repeated for QTL detection in all
331 traits scored. The genetic linkage maps and QTL data were graphically represented using
332 MapChart 2.2 (Voorrips 2002).

333 ***$F_{2:3}$ phenotypic analysis of LS-IN and CS-SS phenotypes***

334 To validate the genetic and phenotypic effects among QTL loci identified in F_2, we
335 performed the phenotypic analysis in $F_{2:3}$ for LS-IN and CS-SS phenotypes. For this
336 purpose, we have generated an $F_{2:3}$ population comprising 1180 individuals segregating
337 for Morex and *mul2.b* alleles at 2H and 6H QTLs. The $F_{2:3}$ lines were genotyped with at
338 least four CAPS markers linked to the 2H (M269389, M5729, 2560790, and M49460) and
339 two markers linked to 6H (FL277086, and FL42060) QTLs. All $F_{2:3}$ lines were phenotyped
340 for floret number in LSs and SS phenotype in CSs. The combinations of 2H and 6H allele
341 frequencies and the corresponding phenotypic values for the respective genotypes are
342 plotted as box plots. All box plots in this study were generated using BoxPlotR (Spitzer et
343 al. 2014).

344 **Results**

345 ***Lateral spikelet determinacy is relaxed in the multiflorus2.b***

346 Spikelets of barley are commonly determinate structures with a single floret being
347 produced per spikelet on its axis i.e. rachilla. After the first floret formation, the elongation
348 of the rachilla is stopped and the rest of the rachilla remains as a thin, pale yellow colored
349 suppressed structure adaxial to the spikelet (positioned between rachis and palea of the
350 spikelet; **Fig. 1A, B**). This scenario applies to both CS and LSs of all spikelet triplets along
351 the inflorescence axis. However, in the LSs of *mul2.b* mutants, upon initiation of the first
352 floret, the rachilla further elongates which leads to the development of a second floret at
353 the articulation junction of the elongated rachilla (**Fig. 1A, C**). In *mul2.b* mutants, the
354 elongated rachilla becomes visible on the adaxial side of the second floret (**Fig. 1C**). Often
355 the elongated rachilla on the second floret of *mul2.b* LSs is enlarged, pale green-colored,
356 indicating that the rachilla elongation is not completely abolished after the second floret

357 formation. In line with this, the rachilla in *mul2.b* LS occasionally elongates beyond the
358 second floret and bears a third floret (**Fig. 1D**). Thus, the rachilla elongation suppression
359 in LSs appears to be lost in *mul2.b* rendering the lateral spikelets indeterminate, a feature
360 reminiscent of indeterminate wheat spikelets (**Fig. 1E**). The rachilla elongation and
361 formation of second and third florets were predominantly restricted to the basal half of
362 the spike (**Fig. 1A**)
363
364 To understand the developmental events during the rachilla primordium initiation and
365 elongation, we undertook scanning electronic microscopy (SEM) analysis initially in wild-
366 type progenitor Montcalm. The general barley spike meristem developmental
367 progression starts with the transition of vegetative shoot apical meristem into
368 reproductive inflorescence meristem (IM). The IM initiates spikelet ridge meristem that
369 further differentiates into one central (CSM) and two lateral spikelet meristems (LSM),
370 followed by the formation of two glume primordia in the flanks of each spikelet meristem
371 (Koppolu and Schnurbusch 2019). At this point, in Montcalm we observed that the floret
372 meristem (FM) first differentiates lemma primordium on the abaxial side. After the
373 initiation of lemma primordium, the adaxial side of the floral meristem buds-off to initiate
374 the rachilla primordium (**Fig. 2A**). Later the residual floral meristem is consumed into the
375 initiation of lodicule, stamen, and carpel primordia (**Fig. 2B-E**). The turn of meristem
376 differentiation events is identical in both CSM and LSM. However, visualizing rachilla
377 primordium in CSM is technically challenging especially at the very early stages of spike
378 meristem development due to the acute angle between CSM and the axis of the spike
379 meristem. Hence, we followed the rachilla primordium development in LSs that are
380 positioned away from the spike meristem axis at appropriate floral primordia initiation
381 time points. In general, the organ primordia differentiated from the floret meristem of
382 Montcalm tended to grow normally with an apparent increase in size over the immature
383 spike developmental phases analyzed (**Fig. 2A-E**). However, the rate of rachilla
384 primordium growth appeared to be slowed down compared to other organ primordia
385 differentiated from the FM (**Fig. 2A-E**). At around W5.0 (central spikelet staging), the
386 rachilla is barely visible in the lateral spikelets at the base and middle of the spike (the
387 developmentally advanced portion of the spike; **Fig. 2C**). Later on, during the spike
388 growth period, the rachilla ceases to grow and remains as a suppressed structure in
389 Montcalm (**Fig. 1A, B**). In the *mul2.b* mutant, the rachilla primordium was initiated after
390 the differentiation of lemma primordium similar to Montcalm (**Fig. 2F**). Nevertheless, the

391 rachilla primordium of *mul2.b* LSs was not retarded in development and continued to
392 increase in size along with other floral organs differentiated from floret meristem (**Fig.**
393 **2F-K**). Over different phases of immature spike development, the rachilla primordium
394 elongated further to form a second FM (**Fig. 2I**). Importantly, the rachilla elongation and
395 formation of additional FM in *mul2.b* was restricted to the LSs; whereas, the rachilla of CS
396 remained as a suppressed structure (**Fig. 2K**).
397
398 Since the LSs of *mul2.b* mutants produced additional florets that are frequently fertile and
399 grain-bearing, we evaluated various yield and biomass-related traits in *mul2.b* and
400 Montcalm. Even though the LSs of *mul2.b* developed more florets per spikelet, a
401 significantly increased maximum yield potential was observed in *mul2.b* compared to
402 Montcalm (Median spikelet number at W8.0, Montcalm 88.5 spikelet primordia; *mul2.b*
403 102 spikelet primordia; p-value: 5.07E-13). However, the number of fertile spikelets were
404 significantly lowered in *mul2.b* (Median fertile spikelets – 39 in *mul2.b*, 45 in Montcalm;
405 p-value: 0.001) probably owing to the enhanced sink strength in the basal half of the spike
406 and consequent post-anthesis growth abortion of spikelets in the apical part of the spike
407 (**Fig. S1A-C**). The grain parameters such as thousand-grain weight (TGW), grain area
408 (GrA), width (GW) and length (GL) did not show significant differences between
409 Montcalm and *mul2.b* when grains from CS and LS were analyzed together (**Fig. S2A-D**).
410 However, the differences for these traits became apparent between Montcalm and *mul2.b*
411 when the CS and LS grains were measured separately. Interestingly the TGW of CS grains
412 was significantly increased in *mul2.b* (p-value: 0.020) due to the slight increase in grain
413 area, mainly contributed by the increase in GW (**Fig. S2E-H**). The TGW of LSs did not show
414 a significant difference between Montcalm and *mul2.b* (**Fig. S2I**). The parameters GW and
415 GL followed opposite tendencies in *mul2.b* LSs where GW was slightly higher and GL was
416 significantly lowered (p-value: 3.61E-05) compared to Montcalm, probably leading to
417 indifferent GrA and TGW (**Fig. S2I-L**). Apart from the grain parameters, the plant height
418 was significantly reduced in *mul2.b* (p-value: 0.020), whereas the number of tillers
419 including productive spike-bearing tillers and unproductive tillers remained indifferent
420 (**fig. S1D-G**).
421
422 ***Lateral spikelets of mul2.b display a gradual rachilla elongation phenotype***
423 The extent of rachilla elongation and the type of additional structures being formed in the
424 LSs of *mul2.b* varied among spikelets of each spike. To quantify these additional

425 structures, we devised a score to classify them into four phenotype component classes
426 such as *mul2 – class I* (*mul2-I*), *mul2-II*, *mul2-III*, and *mul2-IV*. The *mul2-I* had the strongest
427 LS rachilla elongation phenotype with the formation of a second floret that is often fertile
428 and an occasional third floret (**Fig. 3B, C,** and **Fig. S3B**). Also, the second floret with an
429 elongated awn is part of the *mul2-I* class. The reproductive organ development is mostly
430 complete in *mul2-I* except for the occasional lack of carpel growth. The second floret of
431 *mul2-II* is comparatively smaller without awn elongation (**Fig. 3D, E** and **Fig. S3C**).
432 Occasionally, the second floret in the *mul2-II* class had stamens but carpel growth is
433 completely abolished. In the *mul2-III* class, the unsuppressed rachilla showed bi- or
434 trifurcation at the base that further elongated into a thin and long filament-like structure
435 (**Fig. 3F, G** and **Fig. S3D**). The *mul2-IV* phenotypic class is similar to *mul2-III* except that
436 the unsuppressed rachilla did not elongate into a filament-like structure (**Fig. 3H, I** and
437 **Fig. S3E**). In both *mul2-III*, and *-IV* the elongated rachilla did not attain a second floret
438 identity as seen in *mul2-I* and *mul2–II*. The spatial occurrence of *mul2-I, -II, -III, -IV*
439 individual component classes did not show any preferential pattern in the spike indicating
440 the random nature of their occurrence along the spike axis (**Fig. S4**). Throughout this
441 report, we referred to the rachilla elongation phenotype of LSs as lateral spikelet
442 indeterminacy (LS-IN).
443
444 ***mul2.b mutation promotes supernumerary spikelet formation in central spikelets***
445 In contrast to the loss of spikelet determinacy in the LSs, the *mul2.b* mutant showed
446 another interesting feature, i.e. the formation of supernumerary spikelets (SS) exclusively
447 in the CS. The SSs were formed abaxial to the typical CSs (**Fig. 1F**). The observed
448 supernumerary spikelet phenotype in *mul2.b* ranged from the formation of rudimentary
449 floral bract-like structures to complete spikelets with occasional grain formation (**Fig.
450 1F**). Such a SS phenotype is also evident in the barley mutant *extrafloret.a* (BM-NIL(*flo.a*).
451 Interestingly, the SSs that originated at the CSs were occasionally indeterminate with
452 rachilla elongation and formation of second floret similar to the indeterminate LS
453 phenotype in *mul2.b* (**Fig. 1F**). In this report, we termed the SS phenotype on the CS as
454 "CS-SS".
455
456 ***Genetic mapping identifies genomic regions responsible for the LS-IN and CS-SS***
457 ***phenotypes***

458 Previous studies reported that the LS-IN trait in *mul2.b* showed a monogenic recessive
459 inheritance pattern (Walker et al. 1963). Hence, we developed two F_2 mapping
460 populations by crossing *mul2.b* with Morex (Morex × *mul2.b*; POP 2014-1) and Montcalm
461 (*mul2.b* × Montcalm; POP 2014-2) for genetic mapping. Of the 163 F_2 lines phenotyped
462 from POP 2014-1, 35 and 83 F_{2s} showed strong and weak to moderate LS-IN phenotypes,
463 respectively, while 45 F_{2s} were WT, suggesting that the observed phenotype segregation
464 was in contradiction with the previously proposed monogenic recessive inheritance
465 pattern for the LS-IN trait (Walker et al. 1963). From our phenotypic analysis, the LS-IN
466 phenotype appeared to follow an incomplete dominance with homozygous mutant F_{2s}
467 showing strong and the heterozygous F_{2s} showing weak to moderate LS-IN phenotypes
468 ($\chi 2$ = 0.591, *p-value* = 0.442). A similar incomplete dominant inheritance was also
469 observed for the POP 2014-2 (**Supplementary Table 2**). With respect to the CS-SS
470 phenotype, 99 F_{2s} of POP 2014-1 showed the phenotype whereas 64 F_{2s} did not show a
471 phenotype; and hence, were wild type for CS-SS. The majority of the F_{2s} with CS-SS
472 phenotype also had the LS-IN phenotype (70 out of 99 F_{2s}), while 29 F_{2s} that were wild
473 type for LS-IN also showed a weak CS-SS phenotype. Thus, the phenotypic inheritance
474 analysis in F_{2s} indicated that the *mul2.b* phenotype is in fact a combination of LS-IN and
475 CS-SS phenotypes.
476
477 For identifying the genomic region(s) harboring the *mul2.b* mutation, we adopted
478 sequencing-based bulked-segregant analysis by exome capture (Mascher et al. 2014;
479 Mascher et al. 2013). To this end, DNAs from 27 mutant F_{2s} with a strong LS-IN phenotype,
480 of which 20 individuals also had the CS-SS phenotype (**Figure 4A**), and 25 wild-type F_{2s}
481 were pooled to form the LS-IN/CS-SS mutant and wild-type bulks. The two bulks were
482 subjected to exome capture and subsequently sequenced on Illumina Hiseq2000. The
483 single nucleotide polymorphisms were identified by mapping sequence reads onto the
484 Morex reference genome. The SNP allele frequencies from the two pools were visualized
485 along the barley physical and genetic maps. Surprisingly, the allele frequency distribution
486 showed two distinct peaks on chromosomes 2H and 6H where in both cases the mutant
487 allele frequencies for the combined LS-IN/CS-SS phenotype increased over 75% and wt
488 allele frequency dropped to about 25% (**Fig. 4B**).
489
490 ***A novel locus regulates the CS-SS phenotype in mul2.b***

491 In our BSA, allele frequencies peaked on 2H and 6H, indicating that the combined
492 phenotypes of LS-IN and CS-SS are regulated by two independent loci in *mul2.b*. Previous
493 genetic analyses linked the *flo.a* phenotype on the short arm of 6H (Druka et al. 2011).
494 Interestingly, the CSs of the barley BM-NIL(*flo.a*) mutant showed the identical CS-SS
495 spikelet phenotype as *mul2.b* (**Fig. 5A-B**), providing the possibility that both loci might be
496 identical. To examine this idea (**Fig. 5A-B**), we made reciprocal crosses between these
497 two mutant loci to evaluate allelism between them. The CS-SS phenotype in *flo.a* was
498 previously shown to follow a monogenic recessive inheritance (Gustafson 1969). All true
499 F_{1s} generated from the *mul2.b* and BM-NIL(*flo.a*) crosses showed a strong CS-SS
500 phenotype (**Fig. 5A-C**), potentially suggesting that the CS-SS phenotype in both BM-
501 NIL(*flo.a*) and *mul2.b* is regulated by a single locus. However, evidence can only be
502 provided by checking phenotypes of F_{2s}. We therefore evaluated the F_2 generation of the
503 BM-NIL(*flo.a*) × *mul2.b* cross for the CS-SS phenotype to further verify the potential allelic
504 relation of *flo.*a and *mul2.b*. Surprisingly, we found segregation for the CS-SS phenotype
505 among the F_2 progenies: i.e. of the 395 F_{2s} analyzed, 106 did not show the CS-SS
506 phenotype, whereas 289 F_{2s} showed a very weak to very strong CS-SS phenotype (**Fig.
507 5D**). The observed phenotype segregation in F_2 thus indicated that the CS-SS phenotype
508 in *mul2.b* and *flo.a* is most likely regulated by two-independent loci(**Fig. 5E**). The allele
509 and phenotype proportion analysis for the BM-NIL(*flo.a*) × *mul2.b* dihybrid cross showed
510 that the 6H locus regulating the CS-SS phenotype in *mul2.b* followed a recessive
511 inheritance ($\chi 2 = 3.859$, *p-value* = 0.0495). From our exome capture data, the highest allele
512 frequency difference for the 6H peak lied between 59.92 – 61.05 cM (POPSEQ position),
513 whereas the *flo.a* locus was mapped to 52.20 cM (data not shown), indicating that the CS-
514 SS phenotypes in *mul2.b* and *flo.a* are regulated by two independent loci on 6H.
515
516 ***Genetic linkage of the LS-IN and CS-SS phenotypes to 2H and 6H***
517 To conduct a rough genetic linkage analysis of the LS-IN and CS-SS phenotypes we
518 selected 11 SNPs on 2H (33.70 – 87.70 cM POPSEQ) and seven SNPs on 6H (31.90 – 92.20
519 cM POPSEQ) based on the introgressions identified from BSA. The SNPs were converted
520 to restriction enzyme-based CAPS markers for genotyping. For SNP marker mapping, we
521 phenotyped 136 new F_{2s} of the Morex × *mul2.b* population in the year 2015 (POP 2015).
522 We knew that the barley spike-branching gene *COM2* is also located on 2H (45.0 cM),
523 mutants of which often displayed the LS-IN phenotype (McKim et al. 2018; Poursarebani
524 et al. 2015). To check if the LS-IN phenotype is regulated by *COM2*, we developed a CAPS

525 marker out of *COM2* for mapping in our population. Different from the phenotyping
526 method followed for POP 2014-1 and POP 2014-2, we quantified the LS-IN phenotype in
527 POP 2015, based on *mul2-I*, *-II*, *-III*, and *-IV* classes (described earlier in results). In the
528 same F_{2s}, we quantified the CS-SS phenotype. Out of 136 F_{2s} phenotyped, 67 showed
529 various quantities of *mul2-I, -II, -III, -IV* LS-IN phenotypes, while 69 were wildtype for LS-
530 IN. This segregation did not fit the incomplete dominant inheritance ($\chi 2 = 48.039$, *p-value*
531 = <0.0001) observed in POP 2014-1 and POP 2014-2, sugesting some sort of plasticity for
532 the LS-IN phenotype. With respect to the CS-SS phenotype, 62 F_{2s} of POP 2014-1 showed
533 the CS-SS, the majority of which also had LS-IN phenotype while 74 were wt for CS-SS.
534
535 For linkage analysis of the LS-IN phenotype, we converted the phenotype quantities
536 (cumulative frequencies of the *mul2-I, -II, -III,* and *-IV* classes) into binary scores along
537 with SNP marker genotypes. However, after comparing the SNP and phenotype marker
538 scores, six out of 136 F_{2s} had a mismatch between phenotype and marker genotypes.
539 These included, two F_{2s} that showed the LS-IN phenotype but had homozygous WT
540 genotype calls and four F_{2s} that were phenotypically wt for LS-IN but had mutant
541 genotype calls at the majority of markers mapped on 2H (**Fig. 6A**). The two F_{2s} that had
542 wt genotype calls on 2H showed a weak LS-IN phenotype (*mul2-III* and *-IV*; **Fig. 6A**).
543 However, performing linkage analysis of the LS-IN phenotype and genotype scores by
544 excluding the six conflicting F_{2s}, linked LS-IN in between markers M1865727 and M5729
545 away from the *COM2* gene (**Fig. 6B**). Since the LS-IN phenotype was measured in a
546 quantitative manner, we were also able to perform QTL analysis for the LS-IN phenotype
547 (cumulative *mul2.b-I, -II, -III, and -IV*) together with CAPS marker data from 2H and 6H.
548 Expectedly based on our previous exome capture data, LS-IN showed a major QTL on 2H
549 with marker M5729 explaining the highest phenotypic value (**Fig. 6C, E**). However, we
550 also noticed another major QTL for the LS-IN phenotype on 6H with FL209450 explaining
551 the highest phenotypic value (**Fig. 6C, E**). Furthermore, our QTL analysis of the CS-SS
552 phenotype with marker data from 2H and 6H showed a single major QTL on 6H (**Fig. 6D-**
553 **E**). Most interestingly, the CS-SS QTL co-located with the QTL region identified for LS-IN
554 on 6H (**Fig. 6C-E**), indicating that the 6H locus may regulate both phenotypes—CS-SS and
555 LS-IN.
556
557 ***Whole-genome QTL analysis reveals more and novel genetic factors conditioning the***
558 ***LS-IN and CS-SS phenotypes***

559 Since our partial-genome QTL analysis of LS-IN and CS-SS in the Morex × *mul2.b*
560 population (POP 2015) indicated that these phenotypes are probably inherited in a
561 quantitative fashion, we intended to perform whole-genome QTL analysis in the Morex ×
562 *mul2.b* F_2 population. To this end, we screened another ~1,000 F_{2s} with markers M9646
563 and M41923 on 2H that are spaced apart by 37.8 cM (**Fig. 6B**). Between these two
564 markers, we selected 177 recombinant individuals as an independent F_2 population (POP
565 2016). We quantified their LS-IN and CS-SS phenotypes by counting the instances of LS-
566 IN (cumulatively, number of *mul2-I, -II, -III,* and *-IV* classes) and CS-SS (extra central
567 spikelets) per plant.
568
569 The LS-IN phenotype scored in POP 2016 fitted an incomplete dominant inheritance
570 mode as observed in POP 2014-1 ($\chi 2 = 0.092$; p-value = 0.761). With respect to the CS-SS
571 phenotype in POP 2016, 38 F_{2s} did not show a phenotype, whereas 138 F_{2s} carried the CS-
572 SS phenotype. The majority of the F_{2s} harboring the CS-SS phenotype also had the LS-IN
573 phenotype (104 F_{2s}). The frequencies of phenotype distributions were also skewed for the
574 LS-IN and CS-SS phenotypes, indicating that these traits were not strictly polygenic (**Fig.**
575 **S5**). In spite of that, we proceeded analyzing LS-IN and CS-SS as quantitative traits, since
576 we had observed two QTLs (on 2H and 6H chromosomes) for the LS-IN trait in the POP
577 2015. For the QTL analysis of F_{2s} in POP 2016, we normalized the phenotypic value of both
578 traits (LS-IN and CS-SS) by estimating BLUEs to have a more meaningful view of the
579 phenotypes on a per spike basis.
580
581 The 177 F_{2s} from POP 2016 were subjected to the GBS pipeline at IPK to generate SNP
582 marker data. From our GBS analysis we got data for 1,573 SNP markers. The low number
583 of polymorphic markers from this population can be attributed to the high genetic
584 similarity of the mapping genotypes Morex and Montcalm (progenitor of *mul2.b* mutation;
585 **Fig. S6**). Upon filtering for markers with >10% missing data or two or more linked
586 markers without recombination across F_{2s}, we mapped 605 markers onto 11 linkage
587 groups. The barley chromosome 3H was split into three linkage groups, whereas 5H, 7H
588 were split into two linkage groups due to lack of marker coverage mainly in the
589 centromeric regions. Chromosomes 1H, 2H, 4H, and 6H formed unique linkage groups
590 (**Fig. S6**). The genotypic and phenotypic data were used for QTL detection using Genstat
591 19.
592

593 Similar to the QTLs identified from POP 2015, we identified two major QTLs for LS-IN
594 (cumulative *mul2.b-I, -II, -III, and -IV*) on 2H (termed *QMUL2.I-IV.ipk-2H*; -log10(P)–24.70;
595 %PVE–32.19) and 6H (*QMUL2.I-IV.ipk-6H*; -log10(P)–10.93; %PVE–13.50) (**Fig. 7; Table**
596 **1**) in POP 2016. We also performed QTL analysis for the LS-IN component classes *mul2.b-*
597 *I, -II, -III, and –IV* separately to further dissect the genetic basis of the individual phenotype
598 classes. For the *mul2-I, -II,* and *-III* classes major QTLs were detected on 2H and 6H which
599 co-located with *QMUL2.I-IV.ipk-2H* and *QMUL2.I-IV.ipk-6H* (**Fig. 7; Table 1**). For the
600 weakest LS-IN component class - *mul2.b-IV*, only the 2H QTL co-located with both LS-IN
601 cumulative and component QTLs on 2H while the 6H QTL was not detected for this class
602 (**Fig. 7; Table 1**). Apart from the 2H and 6H QTLs for the *mul2.b-III* LS-IN component class,
603 we identified two minor QTLs, *QMUL2.III.ipk-3H(1)* and *QMUL2.III.ipk-3H(2)* on 3H(1) and
604 3H(2) linkage groups explaining 8.43% and 5.65% of the observed phenotypic variation
605 (**Fig. 7; Table 1**). Notably, in four out of five QTLs detected for the LS-IN trait the high
606 phenotype value allele was derived from the *mul2.b* mutant parent; except for
607 *QMUL2.III.ipk-3H(2)*, here the high-value allele was derived from Morex (**Fig. S9**).
608
609 For the CS-SS trait a single major QTL on 6H was identified (*QMUL2.SS.ipk-6H*; -log10(P)–
610 26.38; %PVE – 47.11; **Fig. 7; Table 1**). Interestingly, *QMUL2.SS.ipk-6H* co-located with
611 *QMUL2.I-IV.ipk-6H* and also with the 6H QTLs for LS-IN component classes, *mul2-I, -II,* and
612 *-III* (**Fig.7**), indicating that a single genetic factor may underlie the LS-IN and CS-SS QTLs
613 on 6H. We also found a minor QTL for the CS-SS trait on 5H(2) - *QMUL2.AS.ipk-5H(2)*
614 explaining 4.32% of phenotypic variation (**Fig. 7; Table 1**). Interestingly, the high
615 phenotype value allele for *QMUL2.AS.ipk-5H(2)* originated from the Morex parent (**Fig.**
616 **S10**). Thus, the Morex-derived high phenotype value alleles of minor QTLs, *QMUL2.III.ipk-*
617 *3H(2)* and *QMUL2.AS.ipk-5H(2)* for LS-IN and CS-SS showed that independent genetic
618 factors responsible for controlling these traits are present in both parents of the Morex ×
619 *mul2.b* cross.
620
621 ***QTL allele effects for the LS-IN and CS-SS phenotypes***
622 To estimate the phenotypic effect contributed by QTL alleles for the LS-IN trait, we
623 evaluated combinations of Morex ("MM"), *mul2.b* (allele "*mm*"), and Morex/*mul2.b* (alleles
624 "*M/m*") alleles at *QMUL2.I-IV.ipk-2H* and *QMUL2.I-IV.ipk-6H* QTLs in F_2. Interestingly, the
625 strongest mutant LS-IN phenotype (cumulative *mul2.b-I, -II, -III, and -IV*) was manifested
626 only in F_{2s} with mutant "*mm*" alleles present in both QTL loci (**Fig. S7A**). The LS-IN

627 phenotypic effect got drastically reduced in F_{2s} with alleles "*mm*" and "*MM*" at 2H and 6H
628 QTLs, respectively (**Fig. S7A**). Also heterozygosity at both QTL loci in combination with
629 the respective mutant "*mm*" allele [e.g. *mm*(2H)/*Mm*(6H); or *Mm*(2H)/*mm*(6H)]
630 enhanced LS-IN phenotype in comparison with the wild type allele combination, [(e.g.
631 *mm*(2H)/*MM*(6H) or *MM*(2H)/*mm*(6H)] indicating that *QMUL2.I-IV.ipk-6H* enhanced
632 *QMUL2.I-IV.ipk-2H* effect in an additive manner (**Fig. S7A**). The single major QTL for the
633 CS-SS trait (*QMUL2.SS.ipk-6H*), however, was not influenced by the alleles at *QMUL2.I-*
634 *IV.ipk-2H*, indicating that the CS-SS trait is majorly controlled by 6H QTL **(Fig. S7B**).
635 Similar phenotypic effects for LS-IN and CS-SS traits were also observed in $F_{2:3}$ generation
636 (**Fig. S8**), indicating the stable inheritance of these phenotypes.
637
638 The LS-IN component trait *mul2.b-III* had two major QTLs, one on 2H (*QMUL2.III.ipk-2H*)
639 and 6H (*QMUL2.III.ipk-6H*) but also two minor QTLs on 3H (*QMUL2.III.ipk-3H(1)*,
640 *QMUL2.III.ipk-3H(2)*). Interestingly, the phenotypic effect was highly enhanced in F_{2s} with
641 favorable QTL alleles at these four loci, i.e. *mul2.b* allele at 2H, 6H, 3H(1) QTLs, and Morex
642 allele at 3H(2) QTL, indicating the additivity of these loci (**Fig. S9**). Also for the CS-SS trait,
643 a similar additive phenotype was observed in F_2 lines carrying high phenotype value
644 alleles at *QMUL2.SS.ipk-6H* (*mul2.b* alleles) and *QMUL2.SS.ipk-5H(2)* (Morex alleles) loci
645 (**Fig. S10**).
646
647 **Discussion**
648 ***Mutations in multiflorus.2b induce two ancestral phenotypes – LS-IN and CS-SS***
649 The spikes of the *Triticeae* tribe are proposed to be derivatives of ancestral compound
650 spike/panicle inflorescences obtained through an evolutionary series of inflorescence
651 branch complexity reduction (Koppolu and Schnurbusch 2019; Perreta et al. 2009;
652 Vegetti 1995). Within Triticeae species, spike inflorescences show structural differences
653 in terms of determinacy at the levels of the spike (presence or absence of terminal
654 spikelet) and spikelet (uni- or multi-floreted spikelet) (Sakuma et al. 2011). Uni-floreted
655 condition is manifested due to suppression of rachilla elongation after the initiation of the
656 first floret, whereas in multi-floreted spikelets rachilla elongation continues to generate
657 more florets. Two peculiar Triticeae species with contrasting determinacy features at
658 both levels include barley (determinate spikelet, indeterminate spike) and wheat
659 (determinate spike, indeterminate spikelet). It was proposed that terminal spikelet
660 identity (determinate spike) and multi-floreted conditions (indeterminate spikelet) of

661 wheat are ancestral whereas indeterminate spike and uni-floreted (determinate spikelet)
662 conditions are derived features in barley (Clayton 1990; Zhong et al. 2021). The mutants
663 of barley *mul2.b* lost the spikelet determinacy producing ancestral multi-floreted
664 condition similar to wheat spikelets, but the derived spike indeterminacy character is
665 retained. Interestingly the multi-floreted condition was restricted to LS of *mul2.b* (LS-IN)
666 with CSs retaining the determinate character. Such determinacy differences between CS
667 and adjacent LSs could be probably due to separate genetic factors controlling this
668 condition in CS and LS differently.
669
670 Notably, mutants of *mul2.b* also produce supernumerary spikelets (SS) in the CS (CS-SS).
671 The SS feature appears to be analogous with the paired spikelet phenotype of wheat and
672 the spikelet pair phenotype characteristic to maize, sorghum, and other *Andropogoneae*
673 species (Boden et al. 2015). Also, species belonging to the Triticeae genera *Crithops* and
674 *Taeniatherum* bear two spikelets at each rachis node on the spike (Frederiksen and
675 Seberg 1992), probably indicating that the mechanism regulating SS phenotype is an
676 ancestral feature retained in some of the *Triticeae* species. However, the CS-SS phenotype
677 in *mul2.b* and *flo.a* could be potentially a revertant ancestral phenotype due to mutations
678 in respective loci.
679
680 ***LS-IN and CS-SS are quantitatively inherited in the Morex × mul2.b* cross**
681 Based on our in-depth phenotypic analysis we showed that the *mul2.b* phenotype is a
682 combination of rachilla elongation in LSs (LS-IN) and supernumerary spikelet formation
683 in CSs (CS-SS). The previous genetic and phenotypic analyses involving *mul2.b* apparently
684 did not consider the CS-SS phenotype in central spikelets. Also, the LS-IN phenotype was
685 not evaluated in sufficieent detail probably owing to the difficulty in visualizing the
686 rachilla elongation in lateral spikelets. This might have potentially lead to the
687 classification of *mul2.b* as a monogenic recessive locus (Walker et al. 1963). Our QTL
688 analysis based on comprehensive LS-IN and CS-SS phenotypes revealed two major QTLs
689 for LS-IN (*QMUL2.I-IV.ipk-2H, QMUL2.I-IV.ipk-6H*) and one major QTL for the CS-SS
690 phenotype (*QMUL2.SS.ipk-6H*) (**Fig. 7; Table 1**). Also, two minor QTLs for LS-IN
691 [*QMUL2.III.ipk-3H(1), QMUL2.III.ipk-3H(2)*] and one for CS-SS phenotype [*QMUL2.SS.ipk-*
692 *5H(2)*] were identified indicating the quantitative nature of the *mul2.b* phenotypes (**Fig.**
693 **7; Table 1**). It should be noted that the cv. Morex (wt parent) occasionally showed mild
694 and infrequent rachilla elongation in LSs as well as supernumerary spikelet formation in

CS (data not shown). Consistent with this, we observed for each trait one minor QTL, *QMUL2.III.ipk-3H(2)* and *QMUL2.SS.ipk-5H(2)*, where the phenotypic high-value allele was derived from Morex (**Fig. 7; Table 1**). Previous genetic analyses in wheat involving the paired spikelet phenotype (analogous to *mul2.b* CS-SS) also reported quantitative variation for this trait (Boden et al. 2015; Dobrovolskaya et al. 2015; Echeverry-Solarte et al. 2014).

Our genetic analysis of LS-IN and CS-SS phenotypes revealed co-locating QTLs on 6H (*QMUL2.I-IV.ipk-6H, QMUL2.SS.ipk-6H*; **Fig. 7**), indicating that these phenotypes are potentially regulated by a single locus on 6H. On top of that, the phenotypic effect of LS-IN QTL on 2H is significantly enhanced by the 6H QTL alleles in an additive manner, without which, the LS-IN phenotypic was drastically reduced (**Fig. S7**). Interestingly, the Bowman near-isogenic line of *mul2.b* (BM-NIL(*mul2.b*); GSHO 2089, BW607) showed a mild LS-IN phenotype, whereas the CS-SS phenotype is completely missing in BM-NIL(*mul2.b*) (**Fig. S11**). Such a mild LS-IN phenotype and lack of CS-SS phenotype in BM-NIL(*mul2.b*) could be probably due to the lack of *mul2.b* 6H introgression from the original mutant that enhances the phenotypic effect of 2H QTL. For the LS-IN phenotype component phenotype class *mul2.b-III* we also identified two minor QTLs on 3H. Thus, our precise phenotype quantification data guided us to genetically dissect genomic regions responsible for various LS-IN phenotypes.

Conclusion

Yield in small grain cereals such as barley and wheat is mainly contributed by the number of grains produced per unit area (Ferrante et al. 2017; García et al. 2015; Sakuma and Schnurbusch 2020; Serrago et al. 2013). The grain number can be improved e.g. either by increasing spikelet number per spike, or enhancing floret fertility within spikelets. Here we characterized a barley mutant, *mul2.b*, that showed multi-floreted spikelets as well as more spikelets per spike (supernumerary spikelet formation). Through our genetic analysis, we identified component QTLs conditioning these two trait phenotypes. Further, we laid the foundation for identifying and characterizing the genetic factors underlying these phenotypes by QTL cloning in the future.

Acknowledgments

The authors thank Udda Lundqvist, Jerome Franckowiak, and Thirulogachandar Venkatasubbu for the insightful discussions on the *multiflorus2.b* mutant. We thank Harold Bockelman (USDA-ARS, USA) for providing the *multiflorus2.b* and Montcalm germplasm. We thank Roopkamal Kaur for help with the data analysis. We thank Corinna Trautewig, Mechthild Pürschel, Angelika Pueschel, and Kerstin Wolf for excellent technical assistance. We are also thankful to Heike Müller and Andreas Bähring for supporting graphical artwork.

Author contributions

R.K. conceptualized the study together with T.S.; T.S. and R.K. jointly supervised the study. R.K. generated mapping populations and established the *mul2.b* phenotyping methodology. R.K. and G.J. conducted phenotypic and genetic analyses. Q.H.M. generated BLUE scores for POP 2016. S.G.M. conducted GBS data analysis for POP 2016. T.R. conducted scanning electron microscopy of immature barley spikes. M.M. conducted exome capture data analysis for POP 2014. R.K. drafted the MS with the help from T.S. All authors read and approved the MS.

References

Amagai Y, Aliyeva AJ, Aminov NK, Martinek P, Watanabe N, Kuboyama T (2014) Microsatellite mapping of the genes for sham ramification and extra glume in spikelets of tetraploid wheat. Genetic Resources and Crop Evolution 61:491-498

Bates D, Mächler M, Bolker B, Walker S (2015) Fitting Linear Mixed-Effects Models Using lme4. Journal of statistical software 67:48

Boden SA, Cavanagh C, Cullis BR, Ramm K, Greenwood J, Jean Finnegan E, Trevaskis B, Swain SM (2015) *Ppd-1* is a key regulator of inflorescence architecture and paired spikelet development in wheat. Nature Plants 1:14016

Bonnett OT (1935) The development of the barley spike. Journal of Agricultural Research 51:451-460

Bonnett OT (1936) The development of the wheat spike. Journal of Agricultural Research 53:445-451

Bonnett OT (1966) Inflorescences of maize, wheat, rye, barley, and oats : their initiation and development / 721. University of Illinois, College of Agriculture, Agricultural Experiment Station

Bull H, Casao MC, Zwirek M, Flavell AJ, Thomas WTB, Guo W, Zhang R, Rapazote-Flores P, Kyriakidis S, Russell J, Druka A, McKim SM, Waugh R (2017) Barley *SIX-ROWED SPIKE3* encodes a putative Jumonji C-type H3K9me2/me3 demethylase that represses lateral spikelet fertility. Nature Communications 8:936

Chuck G, Meeley R, Hake S (2008) Floral meristem initiation and meristem cell fate are regulated by the maize *AP2* genes *ids1* and *sid1*. Development 135:3013-3019

Chuck G, Meeley R, Irish E, Sakai H, Hake S (2007) The maize *tasselseed4 microRNA* controls sex determination and meristem cell fate by targeting *Tasselseed6/indeterminate spikelet1*. Nature Genetics 39:1517-1521

Chuck G, Meeley RB, Hake S (1998) The control of maize spikelet meristem fate by the *APETALA2-like* gene *indeterminate spikelet1*. Genes & Development 12:1145-1154

769 Clayton WD (1990) The spikelet. In: Chapman GP (ed) Reproductive versatility in the grasses.
770 Cambridge University Press, Cambridge, UK
771 Debernardi JM, Lin H, Chuck G, Faris JD, Dubcovsky J (2017) *microRNA172* plays a crucial role in wheat
772 spike morphogenesis and grain threshability. Development 144:1966-1975
773 Dixon LE, Greenwood JR, Bencivenga S, Zhang P, Cockram J, Mellers G, Ramm K, Cavanagh C, Swain
774 SM, Boden SA (2018) *TEOSINTE BRANCHED1* regulates inflorescence architecture and
775 development in bread wheat (*Triticum aestivum* L.). The Plant Cell
776 Dobrovolskaya O, Pont C, Sibout R, Martinek P, Badaeva E, Murat F, Chosson A, Watanabe N, Prat E,
777 Gautier N, Gautier V, Poncet C, Orlov YL, Krasnikov AA, Bergès H, Salina E, Laikova L, Salse J (2015)
778 *FRIZZY PANICLE* drives supernumerary spikelets in bread wheat. Plant Physiology 167:189-199
779 Druka A, Franckowiak J, Lundqvist U, Bonar N, Alexander J, Houston K, Radovic S, Shahinnia F,
780 Vendramin V, Morgante M, Stein N, Waugh R (2011) Genetic dissection of barley morphology
781 and development. Plant Physiolology 155:617-627
782 Echeverry-Solarte M, Kumar A, Kianian S, Mantovani EE, Simsek S, Alamri MS, Mergoum M (2014)
783 Genome-Wide Genetic Dissection of Supernumerary Spikelet and Related Traits in Common
784 Wheat. The Plant Genome 7:plantgenome2014.2003.0013
785 Ferrante A, Cartelle J, Savin R, Slafer GA (2017) Yield determination, interplay between major
786 components and yield stability in a traditional and a contemporary wheat across a wide range of
787 environments. Field Crops Research 203:114-127
788 Franckowiak JD (1995) Notes on linkage drag in Bowman backcross derived lines of spring barley.
789 Barley Genetics Newsletter 24:63-70
790 Frederiksen S, Seberg O (1992) Phylogenetic analysis of the Triticeae (Poaceae). Hereditas 116:15-19
791 García GA, Dreccer MF, Miralles DJ, Serrago RA (2015) High night temperatures during grain number
792 determination reduce wheat and barley grain yield: a field study. Global Change Biology 21:4153-
793 4164
794 Greenwood JR, Finnegan EJ, Watanabe N, Trevaskis B, Swain SM (2017) New alleles of the wheat
795 domestication gene *Q* reveal multiple roles in growth and reproductive development.
796 Development 144:1959-1965
797 Jeon J-S, Jang S, Lee S, Nam J, Kim C, Lee S-H, Chung Y-Y, Kim S-R, Lee YH, Cho Y-G, An G (2000) *leafy*
798 *hull sterile1* Is a homeotic mutation in a rice *MADS BOX* gene affecting rice flower development.
799 Plant Cell 12:871-884
800 Kellogg E, Camara P, Rudall P, Ladd P, Malcomber S, Whipple C, Doust A (2013) Early inflorescence
801 development in the grasses (Poaceae). Frontiers in Plant Science 4
802 Komatsuda T, Pourkheirandish M, He C, Azhaguvel P, Kanamori H, Perovic D, Stein N, Graner A, Wicker
803 T, Tagiri A, Lundqvist U, Fujimura T, Matsuoka M, Matsumoto T, Yano M (2007) Six-rowed barley
804 originated from a mutation in a homeodomain-leucine zipper I-class homeobox gene.
805 Proceedings of the National Academy of Sciences 104:1424-1429
806 Koppolu R, Anwar N, Sakuma S, Tagiri A, Lundqvist U, Pourkheirandish M, Rutten T, Seiler C,
807 Himmelbach A, Ariyadasa R, Youssef HM, Stein N, Sreenivasulu N, Komatsuda T, Schnurbusch T
808 (2013) *Six-rowed spike4* (*Vrs4*) controls spikelet determinacy and row-type in barley. Proceedings
809 of the National Academy of Sciences 110:13198-13203
810 Koppolu R, Schnurbusch T (2019) Developmental pathways for shaping spike inflorescence
811 architecture in barley and wheat. Journal of Integrative Plant Biology 61:278-295
812 Lee DY, An G (2012) Two AP2 family genes, supernumerary bract (SNB) and Osindeterminate spikelet
813 1 (OsIDS1), synergistically control inflorescence architecture and floral meristem establishment
814 in rice. Plant J 69
815 Lee DY, Lee J, Moon S, Park SY, An G (2007) The rice heterochronic gene *SUPERNUMERARY BRACT*
816 regulates the transition from spikelet meristem to floral meristem. Plant J 49
817 Li H (2011) A statistical framework for SNP calling, mutation discovery, association mapping and
818 population genetical parameter estimation from sequencing data. Bioinformatics 27:2987-2993
819 Li H (2013) Aligning sequence reads, clone sequences and assembly contigs with BWA-MEM. Preprint
820 at https://arxivorg/abs/13033997

821 Li H, Handsaker B, Wysoker A, Fennell T, Ruan J, Homer N, Marth G, Abecasis G, Durbin R, Subgroup
822 GPDP (2009) The Sequence Alignment/Map format and SAMtools. Bioinformatics 25:2078-2079
823 Lolas IB, Himanen K, Gronlund JT, Lynggaard C, Houben A, Melzer M, Van Lijsebettens M, Grasser KD
824 (2010) The transcript elongation factor *FACT* affects Arabidopsis vegetative and reproductive
825 development and genetically interacts with *HUB1/2*. Plant J 61:686-697
826 Martin M (2011) Cutadapt removes adapter sequences from high-throughput sequencing reads.
827 EMBnetjournal 17:3
828 Mascher M, Gundlach H, Himmelbach A, Beier S, Twardziok SO, Wicker T, Radchuk V, Dockter C, Hedley
829 PE, Russell J, Bayer M, Ramsay L, Liu H, Haberer G, Zhang X-Q, Zhang Q, Barrero RA, Li L, Taudien
830 S, Groth M, Felder M, Hastie A, Šimková H, Staňková H, Vrána J, Chan S, Muñoz-Amatriaín M,
831 Ounit R, Wanamaker S, Bolser D, Colmsee C, Schmutzer T, Aliyeva-Schnorr L, Grasso S, Tanskanen
832 J, Chailyan A, Sampath D, Heavens D, Clissold L, Cao S, Chapman B, Dai F, Han Y, Li H, Li X, Lin C,
833 McCooke JK, Tan C, Wang P, Wang S, Yin S, Zhou G, Poland JA, Bellgard MI, Borisjuk L, Houben
834 A, Doležel J, Ayling S, Lonardi S, Kersey P, Langridge P, Muehlbauer GJ, Clark MD, Caccamo M,
835 Schulman AH, Mayer KFX, Platzer M, Close TJ, Scholz U, Hansson M, Zhang G, Braumann I,
836 Spannagl M, Li C, Waugh R, Stein N (2017) A chromosome conformation capture ordered
837 sequence of the barley genome. Nature 544:427-433
838 Mascher M, Jost M, Kuon J-E, Himmelbach A, Aßfalg A, Beier S, Scholz U, Graner A, Stein N (2014)
839 Mapping-by-sequencing accelerates forward genetics in barley. Genome Biology 15:R78
840 Mascher M, Richmond TA, Gerhardt DJ, Himmelbach A, Clissold L, Sampath D, Ayling S, Steuernagel B,
841 Pfeifer M, D'Ascenzo M, Akhunov ED, Hedley PE, Gonzales AM, Morrell PL, Kilian B, Blattner FR,
842 Scholz U, Mayer KFX, Flavell AJ, Muehlbauer GJ, Waugh R, Jeddeloh JA, Stein N (2013) Barley
843 whole exome capture: a tool for genomic research in the genus *Hordeum* and beyond. The Plant
844 Journal 76:494-505
845 McKim SM, Koppolu R, Schnurbusch T (2018) Barley Inflorescence Architecture. In: Stein N,
846 Muehlbauer GJ (eds) The Barley Genome. Springer International Publishing, Cham, pp 171-208
847 Ohmori S, Kimizu M, Sugita M, Miyao A, Hirochika H, Uchida E, Nagato Y, Yoshida H (2009) *MOSAIC*
848 *FLORAL ORGANS1*, an *AGL6-Like MADS Box* gene, regulates floral organ identity and meristem
849 fate in rice. Plant Cell 21:3008-3025
850 Perreta MG, Ramos JC, Vegetti AC (2009) Development and structure of the grass inflorescence. The
851 Botanical Review 75:377-396
852 Poursarebani N, Seidensticker T, Koppolu R, Trautewig C, Gawroński P, Bini F, Govind G, Rutten T,
853 Sakuma S, Tagiri A, Wolde GM, Youssef HM, Battal A, Ciannamea S, Fusca T, Nussbaumer T, Pozzi
854 C, Börner A, Lundqvist U, Komatsuda T, Salvi S, Tuberosa R, Uauy C, Sreenivasulu N, Rossini L,
855 Schnurbusch T (2015) The genetic basis of composite spike form in barley and 'miracle-wheat'.
856 Genetics 201:155-165
857 Poursarebani N, Trautewig C, Melzer M, Nussbaumer T, Lundqvist U, Rutten T, Schmutzer T, Brandt R,
858 Himmelbach A, Altschmied L, Koppolu R, Youssef HM, Sibout R, Dalmais M, Bendahmane A, Stein
859 N, Xin Z, Schnurbusch T (2020) COMPOSITUM 1 contributes to the architectural simplification of
860 barley inflorescence via meristem identity signals. Nature Communications 11:5138
861 Ramsay L, Comadran J, Druka A, Marshall DF, Thomas WTB, Macaulay M, MacKenzie K, Simpson C,
862 Fuller J, Bonar N, Hayes PM, Lundqvist U, Franckowiak JD, Close TJ, Muehlbauer GJ, Waugh R
863 (2011) *INTERMEDIUM-C*, a modifier of lateral spikelet fertility in barley, is an ortholog of the
864 maize domestication gene *TEOSINTE BRANCHED 1*. Nature Genetics 43:169-172
865 Ren D, Li Y, Zhao F, Sang X, Shi J, Wang N, Guo S, Ling Y, Zhang C, Yang Z, He G (2013) *MULTI-FLORET*
866 *SPIKELET1*, which encodes an AP2/ERF protein, determines spikelet meristem fate and sterile
867 lemma identity in rice. Plant Physiology 162:872-884
868 Ren D, Xu Q, Qiu Z, Cui Y, Zhou T, Zeng D, Guo L, Qian Q (2019) *FON4* prevents the multi-floret spikelet
869 in rice. Plant Biotechnology Journal 17:1007-1009
870 Ren D, Yu H, Rao Y, Xu Q, Zhou T, Hu J, Zhang Y, Zhang G, Zhu L, Gao Z, Chen G, Guo L, Zeng D, Qian Q
871 (2018) 'Two-floret spikelet' as a novel resource has the potential to increase rice yield. Plant
872 Biotechnology Journal 16:351-353

Sakuma S, Golan G, Guo Z, Ogawa T, Tagiri A, Sugimoto K, Bernhardt N, Brassac J, Mascher M, Hensel G, Ohnishi S, Jinno H, Yamashita Y, Ayalon I, Peleg Z, Schnurbusch T, Komatsuda T (2019) Unleashing floret fertility in wheat through the mutation of a homeobox gene. Proceedings of the National Academy of Sciences 116:5182-5187

Sakuma S, Salomon B, Komatsuda T (2011) The domestication syndrome genes responsible for the major changes in plant form in the Triticeae crops. Plant Cell Physiol 52:738-749

Sakuma S, Schnurbusch T (2020) Of floral fortune: tinkering with the grain yield potential of cereal crops. New Phytologist 225:1873-1882

Schnurbusch T (2019) Wheat and barley biology: Towards new frontiers. Journal of Integrative Plant Biology 61:198-203

Serrago RA, Alzueta I, Savin R, Slafer GA (2013) Understanding grain yield responses to source–sink ratios during grain filling in wheat and barley under contrasting environments. Field Crops Research 150:42-51

Simons KJ, Fellers JP, Trick HN, Zhang Z, Tai Y-S, Gill BS, Faris JD (2006) Molecular characterization of the major wheat domestication gene *Q*. Genetics 172:547-555

Spitzer M, Wildenhain J, Rappsilber J, Tyers M (2014) BoxPlotR: a web tool for generation of box plots. Nature Methods 11:121-122

Tanaka W, Toriba T, Ohmori Y, Yoshida A, Kawai A, Mayama-Tsuchida T, Ichikawa H, Mitsuda N, Ohme-Takagi M, Hirano H-Y (2012) The *YABBY G*ene *TONGARI-BOUSHI1* Is Involved in Lateral Organ Development and Maintenance of Meristem Organization in the Rice Spikelet. The Plant Cell 24:80-95

van Esse GW, Walla A, Finke A, Koornneef M, Pecinka A, von Korff M (2017) Six-Rowed Spike3 (VRS3) is a histone demethylase that controls lateral spikelet development in barley. Plant Physiology 174:2397-2408

Vegetti AA, A.M. (1995) Some evolution trends in the inflorescence of Poaceae. Flora 190:225-228

Voorrips RE (2002) MapChart: Software for the graphical presentation of linkage maps and QTLs. Journal of Heredity 93:77-78

Waddington SR, Cartwright PM, Wall PC (1983) A quantitative scale of spike initial and pistil development in barley and wheat. Annals of Botany 51:119-130

Walker GWR, Dietrich J, Miller R, Kasha K (1963) Recent barley mutants and their linkages II. Genetic data for further mutants. Canadian Journal of Genetics and Cytology 5:200-219

Wendler N, Mascher M, Nöh C, Himmelbach A, Scholz U, Ruge-Wehling B, Stein N (2014) Unlocking the secondary gene-pool of barley with next-generation sequencing. Plant Biotechnology Journal 12:1122-1131

Wolde GM, Trautewig C, Mascher M, Schnurbusch T (2019) Genetic insights into morphometric inflorescence traits of wheat. Theoretical and Applied Genetics 132:1661-1676

Youssef HM, Eggert K, Koppolu R, Alqudah AM, Poursarebani N, Fazeli A, Sakuma S, Tagiri A, Rutten T, Govind G, Lundqvist U, Graner A, Komatsuda T, Sreenivasulu N, Schnurbusch T (2017) *VRS2* regulates hormone-mediated inflorescence patterning in barley. Nature Genetics 49:157-161

Zhang T, Li Y, Ma L, Sang X, Ling Y, Wang Y, Yu P, Zhuang H, Huang J, Wang N, Zhao F, Zhang C, Yang Z, Fang L, He G (2017) *LATERAL FLORET 1* induced the three-florets spikelet in rice. Proceedings of the National Academy of Sciences 114:9984-9989

Zhong J, van Esse GW, Bi X, Lan T, Walla A, Sang Q, Franzen R, von Korff M (2021) *INTERMEDIUM-M* encodes an *HvAP2L-H5* ortholog and is required for inflorescence indeterminacy and spikelet determinacy in barley. Proceedings of the National Academy of Sciences 118:e2011779118

923 **Main text figures**

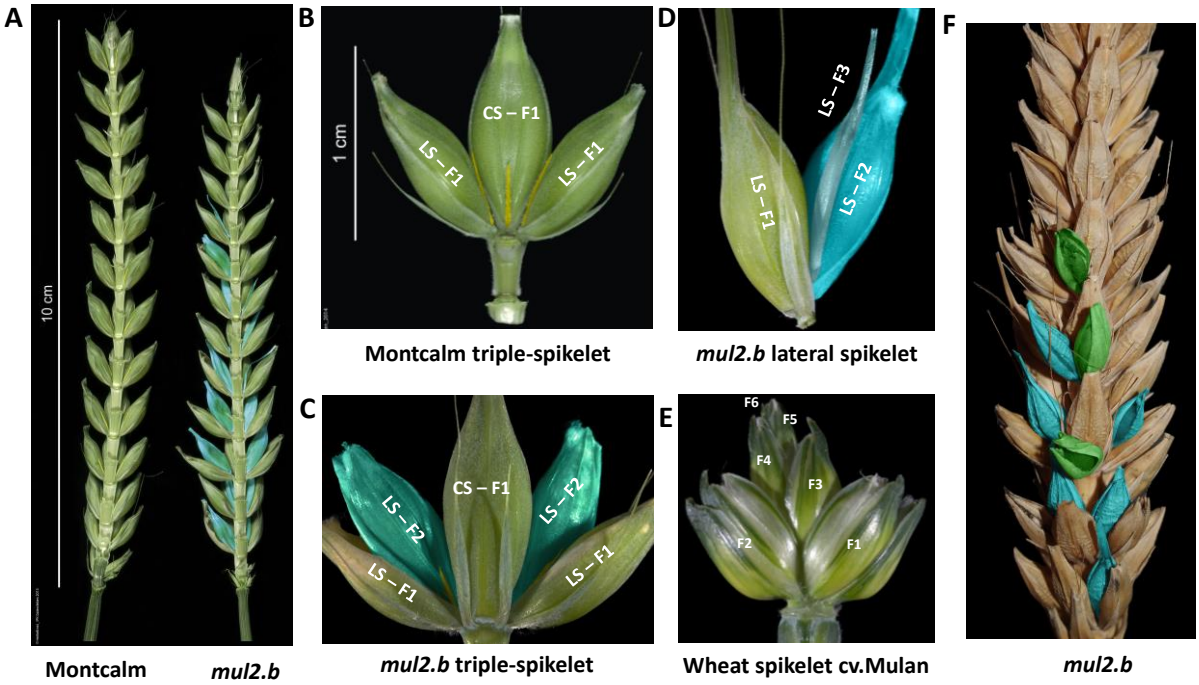

924

925 **Figure 1. Spike and spikelet phenotypes of cv.Montcalm and derived mutant *mul2.b.***
926 (A) cv. Montcalm and *mul2.b* spikes. The dorsal triple spikelet nodes of Montcalm and
927 mul2.b are stripped-off in-order to visualize the rachilla of the lateral spikelets from
928 ventral nodes. The rachilla of lateral spikelets in Montcalm and *the* second floret on the
929 elongated rachilla of *mul2.b* are colored in yellow and turquoise blue respectively. (B)
930 Triple-spikelet node of Montcalm with rachilla of central and lateral spikelets colored in
931 yellow. (C) Triple spikelet node of *mul2.b* mutant showing the formation of the second
932 floret in lateral spikelet nodes (LS-F2). The rachilla on LS-F2 is colored in yellow. (D) The
933 lateral spikelet node of *mul2.b* showing the formation of the second (LS-F2) and third
934 florets (LS-F3). (E) A representative wheat spikelet with six visible florets (F1-F6). (F)
935 *mul2.b* spike showing additional florets in lateral spikelets (blue highlighted) and
936 supernumerary spikelets (green highlighted) on the abaxial side of central spikelets.
937 Awns in all images (except 1E) are clipped-off for better visualization of spikelet features.
938

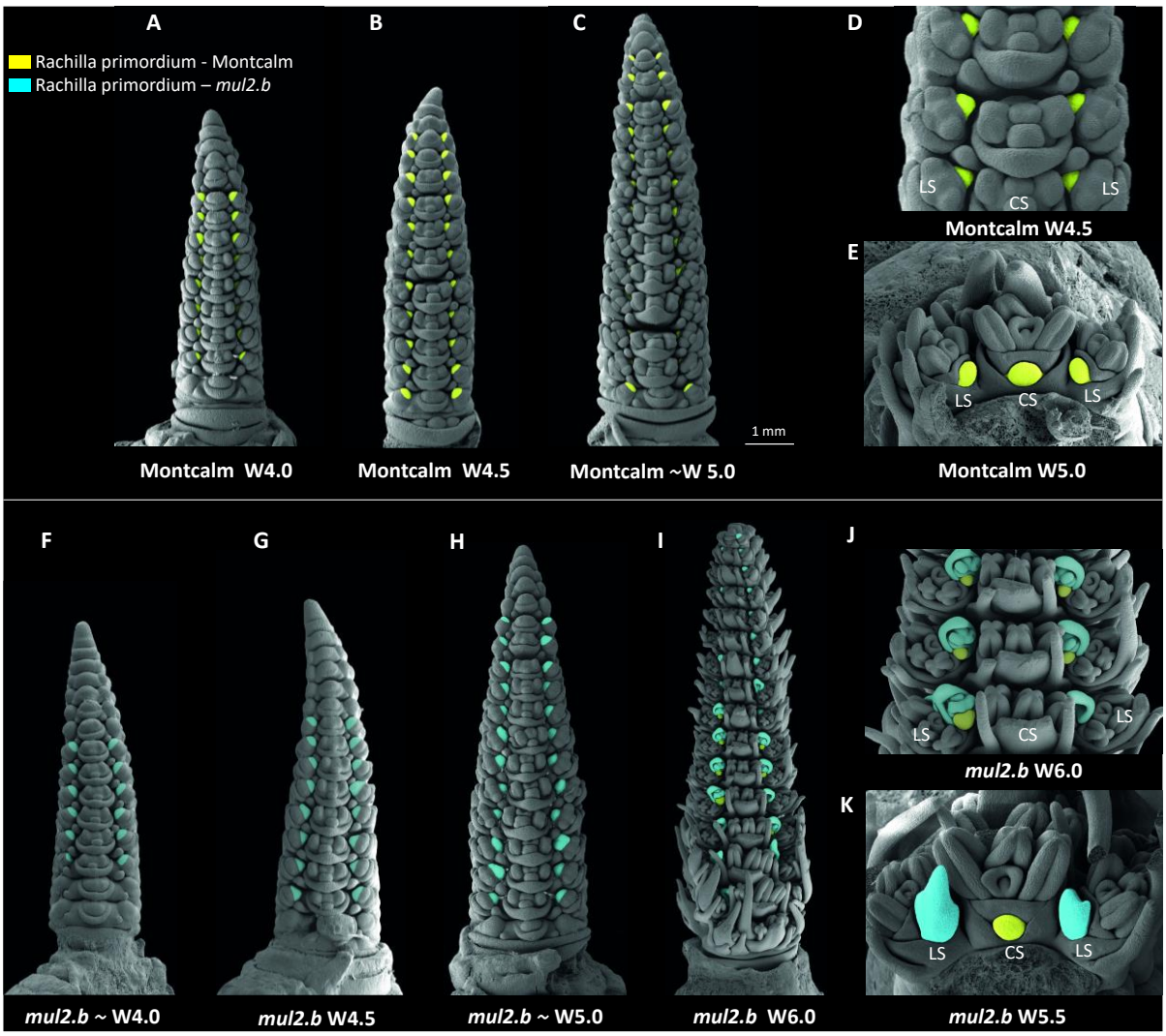

Figure 2. Scanning electron micrographs highlighted with rachilla primordia in Montcalm and derived mutant *mul2.b*.

(A-C) Immature spikes of cv. Montcalm at Waddington W4.0 (A), W4.5 (B), and ~W5.0 (C). (D) Close-up view of three triple-spikelet nodes of Montcalm (E) Top-down view of single triple-spikelet of Montcalm. The lateral spikelet rachilla primordia in figures 2A-E are colored in yellow. (F-I) Immature spikes of *mul2.b* at ~W4.0 (F), W4.5(G), ~W5.0 (H), and W6.0 (I). (J) Close up view of three triple-spikelet nodes of *mul2.b*. (K) Top-down view of single triple-spikelet of *mul2.b*. The rachilla primordium/second floret in lateral spikelets in figures 2F-K are colored in blue. The rachilla primordium seen on the second floret in 2I, 2J, and central spikelet in 2K is colored in yellow. All immature spikes in figure 2 are staged based on the central spikelet development.

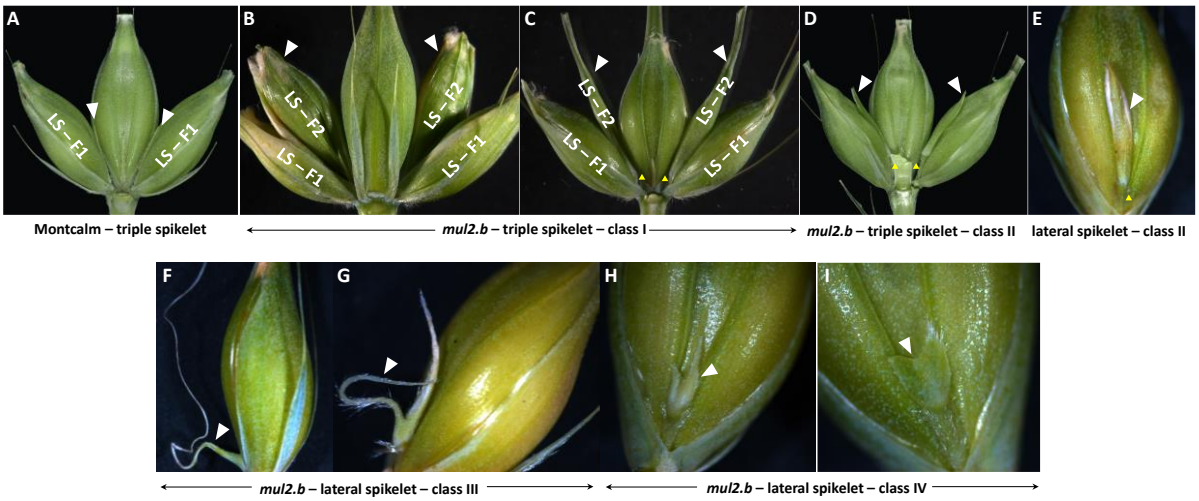

Figure 3. Phenotype classification for lateral spikelet indeterminacy.
(A) Representative spikelet-triplets showing wild-type rachilla of lateral and central spikelets. (B-E) elongated lateral spikelet rachilla developing class I (B, C) and class II additional florets (D, E). (F-G) Class III rachilla elongating into a thin and long filament-like structure. (H-I) Class IV phenotype showing a bifurcated (H) or wedge-shaped rachilla in lateral spikelets (I). Rachilla/additional florets/rachilla malformations in lateral spikelets are indicated with white arrowheads. Yellow arrowheads in figure 3D and E indicate a pedicel below the extra floret in lateral spikelets.

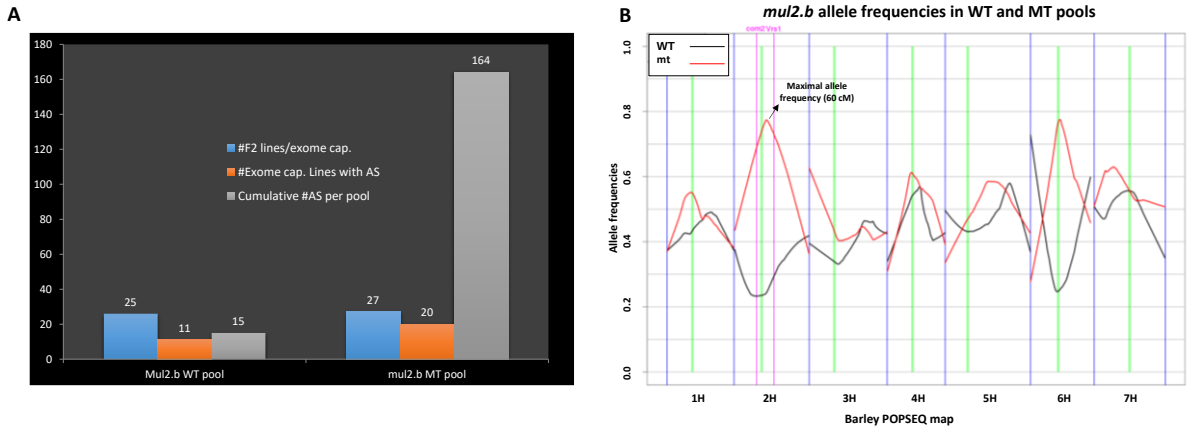

Figure 4. Exome capture-based bulked segregant analysis in Morex × *mul2.b* (POP 2014-1)

Allele frequency plot showing the frequency of wild-type (Morex) and mutant (*mul2.b*) allele distributions across seven barley chromosomes. (B) Graph showing number of F_2 lines per exome capture pool, number of exome capture lines showing supernumerary spikelet phenotype, and strength of supernumerary spikelet phenotype (total supernumerary spikelets per pool) in WT and mt pools.

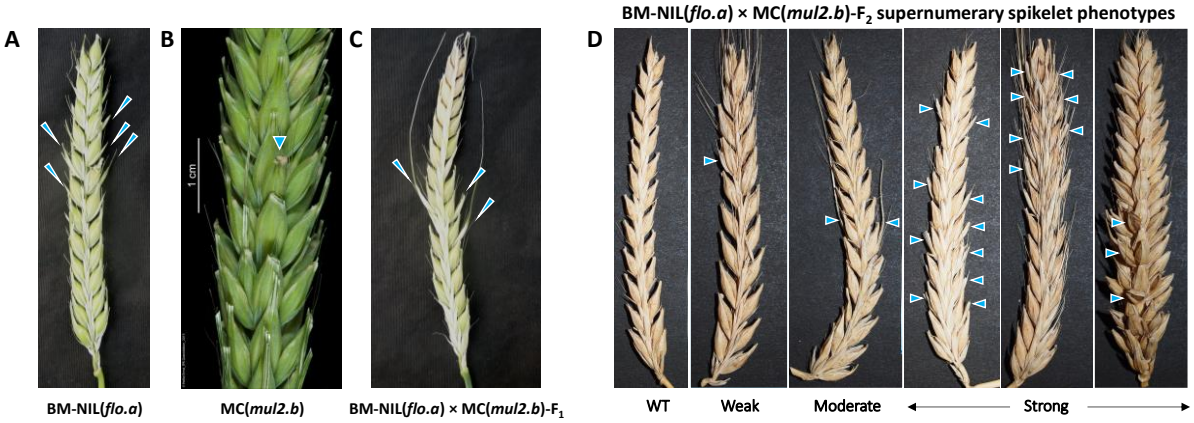

E

BM-NIL(*flo.a*) × MC(*mul2.b*)-F$_2$ supernumerary spikelet phenotypes

Genotype	Allele combination	Dihybrid proportion	ss recessive	SS dominant
FFSS	FF & SS double dominant	1	No	Yes
FFSs	FF dominant + Ss heterozygote	2	No	Yes
FfSS	Ff heterozygote + SS dominant	2	No	Yes
FfSs	Ff & Ss heterozygotes	4	May be	Yes
FFss	FF dominant + ss recessive	1	Yes	No
Ffss	Ff heterozygote + ss recessive	2	Yes	No
ffSS	ff recessive + SS dominant	1	Yes	Yes
ffSs	ff recessive + Ss heterozygote	2	Yes	Yes
ffss	ff & ss double recessive	1	Yes	Yes
Expected lines with mutant phenotype for two genes (%)			68.57%	81.04%
Observed lines with additional spikelet (weak to strong flo.a phenotype)			73.16%	73.16%
Chi-squared (1df)			3.859	15.965
P-value			0.0495	<0.0001

F – Dominant *FLO.A*; S – dominant second supernumerary spikelet locus; f – Recessive *flo.a*; s – recessive second supernumerary spikelet locus; S/s & F/f - Heterozygote

Figure 5. Allelism analysis between *mul2.b* and BM-NIL(*flo.a*).
(A-C) Supernumerary spikelet formation in BM-NIL(*flo.a*) (A), *mul2.b* (B), and the respective F_1 hybrid (C). (D) Supernumerary spikelet phenotypes in BM-NIL(*flo.a*) × *mul2.b* F_2 progenies. (E) Mode of inheritance of supernumerary spikelet phenotype in BM-NIL(*flo.a*) × *mul2.b*. Supernumerary spikelets are indicated by blue arrowheads. F – Dominant *FLO.A*; S – dominant second supernumerary spikelet locus; f – Recessive *flo.a*; s – recessive second supernumerary spikelet locus; S/s & F/f – Heterozygote.

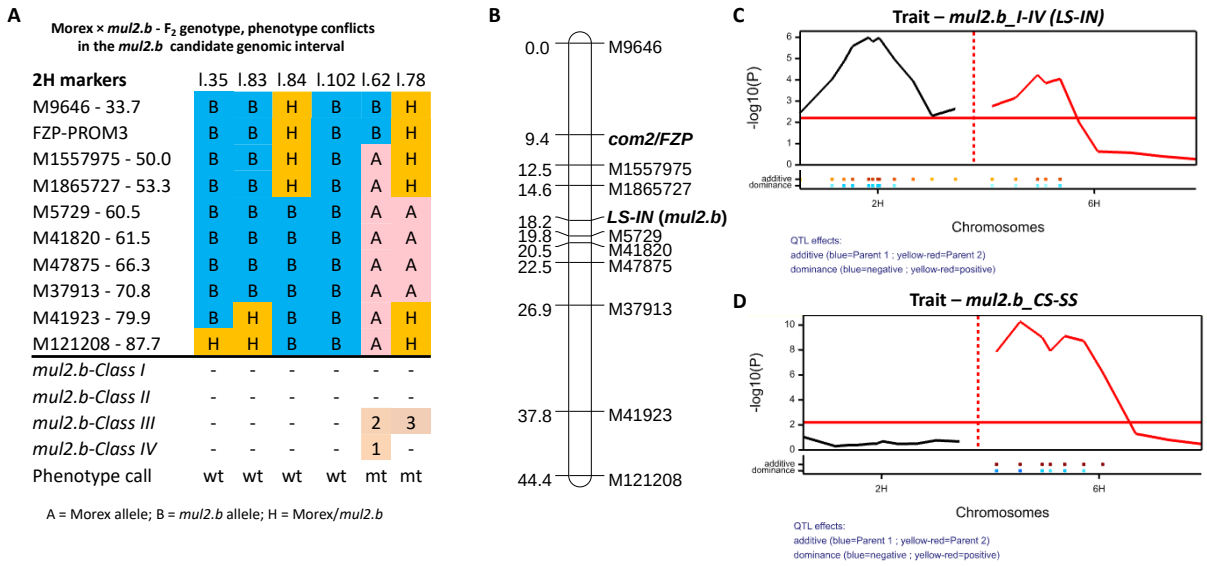

E

Trait	QTL	Chr.	Position (cM)	log10(P)	%Expl. Var.	Add. eff.	High allele	Dom. eff.	Dominant allele
mul2.b_LS-IN	M5729	2H	18.7	5.435	9.565	7.608	*mul2.b*	7.168	Morex
mul2.b_LS-IN	FL209450	6H	12.38	3.945	11.632	8.39	*mul2.b*	6.17	Morex
mul2.b_CS-SS	FL52245	6H	6.41	8.787	21.428	3.352	*mul2.b*	2.944	Morex

Figure 6. Linkage and QTL mapping of LS-IN and CS-SS phenotypes in Morex × *mul2.b* (POP 2015).

(A) The upper panel shows the graphical genotypes of CAPS markers (derived from 2H LS-IN introgression identified from exome capture) that are not fitting with the LS-IN phenotype shown in the lower panel. The linkage map for rachilla elongation/additional floret phenotype after omitting the 6 lines with genotype-phenotype conflicts reported in figure 6A. (C) QTLs for rachilla elongation/additional floret on 2H, 6H chromosomes. (D) QTL for supernumerary spikelet phenotype on the 6H chromosome. (E) Summary of QTLs reported in figures 6C, and D.

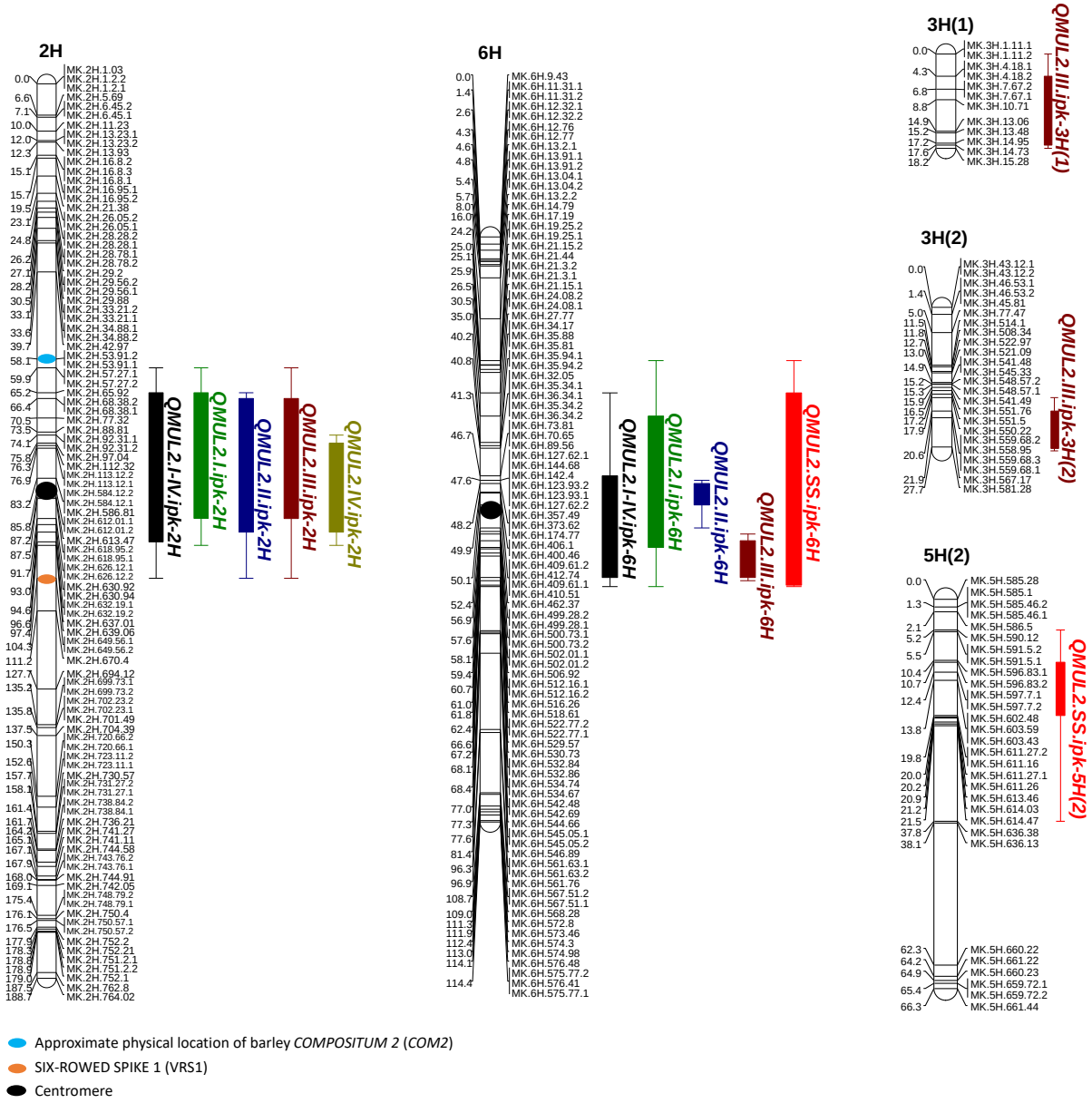

Figure 7. Identified QTLs for LS-IN and CS-SS phenotypes in the Morex × *mul2.b* (POP 2016)

Main text tables

Table 1. List of identified QTLs for LS-IN and CS-SS traits in the Morex × *mul2.b* (POP 2016)

Table 1. List of QTLs identified for LS-IN and CS-SS traits in Morex x mul2.b (POP 1-2016)

Chr.	QTL	Pos (cM)	Sig. Marker	Pos (cM)2	Genetic Interval	-log10(P)	Add. Eff.	High Allele	Dom. Eff.	Dom. Allele	R2 (%)
2H	*QMUL2.I-IV.ipk-2H*	83.00	MK.2H.584.12.1	83.20	75.24 - 90.75	24.70	3.91	mul2.b	2.38	Morex	32.19
6H	*QMUL2.I-IV.ipk-6H*	50.00	MK.6H.409.61.1	50.10	24.72 - 75.27	10.93	2.53	mul2.b	1.49	Morex	13.50
2H	*QMUL2.I.ipk-2H*	79.50	MK.2H.584.12.1	83.20	58.69 - 100.30	10.89	1.61	mul2.b	1.27	Morex	15.20
6H	*QMUL2.I.ipk-6H*	48.00	MK.6H.174.77	48.20	35.36 - 60.63	13.93	1.93	mul2.b	1.56	Morex	21.64
2H	*QMUL2.II.ipk-2H*	83.00	MK.2H.584.12.1	83.20	71.20 - 94.79	15.69	0.32	mul2.b	0.26	Morex	22.83
6H	*QMUL2.II.ipk-6H*	49.00	MK.6H.400.46	49.90	0 - 114	4.36	0.17	mul2.b	-	-	6.57
2H	*QMUL2.III.ipk-2H*	83.00	MK.2H.584.12.1	83.20	74.40 - 91.59	18.75	1.61	mul2.b	0.75	Morex	29.53
6H	*QMUL2.III.ipk-6H*	62.00	MK.6H.522.77.1	62.40	0 - 114	3.88	0.66	mul2.b	-	-	4.98
3H	*QMUL2.III.ipk-3H(1)*	8.00	MK.3H.10.71	8.80	0 - 18	6.41	0.86	mul2.b	-	-	8.43
3H	*QMUL2.III.ipk-3H(2)*	27.00	MK.3H.581.28	27.70	0 - 27	4.44	0.70	Morex	-	-	5.65
2H	*QMUL2.IV.ipk-2H*	83.00	MK.2H.584.12.1	83.20	73.22 - 92.77	11.48	0.60	mul2.b	-	-	26.53
6H	*QMUL2.AS.ipk-6H*	48.00	MK.6H.174.77	48.20	42.97 - 53.03	26.38	1.24	mul2.b	0.73	Morex	47.11
5H(2)	*QMUL2.AS.ipk-5H(2)*	13.00	MK.5H.602.48	13.80	0 - 66	3.76	0.38	Morex	-	-	4.32

Supplementary figures and tables

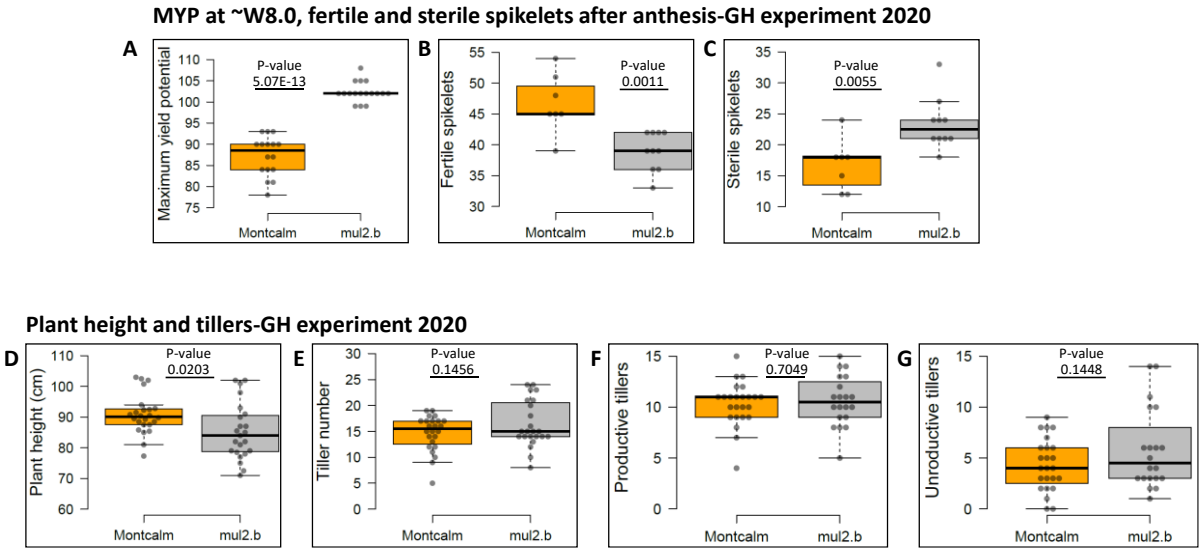

Supplementary figure 1. Spike and biomass-related traits – Montcalm vs. *mul2.b*. (A) Maximum yield potential of Montcalm and *mul2.b* measured before anthesis. (B-C) Fertile grain-bearing spikelets (B) and sterile spikelets (C) at spike maturity. (D-G) Biomass-related traits such as plant height (D) total tillers (E), productive (F), and unproductive (G) tillers. P-values were calculated based on *Student's t-test* (two-tailed).

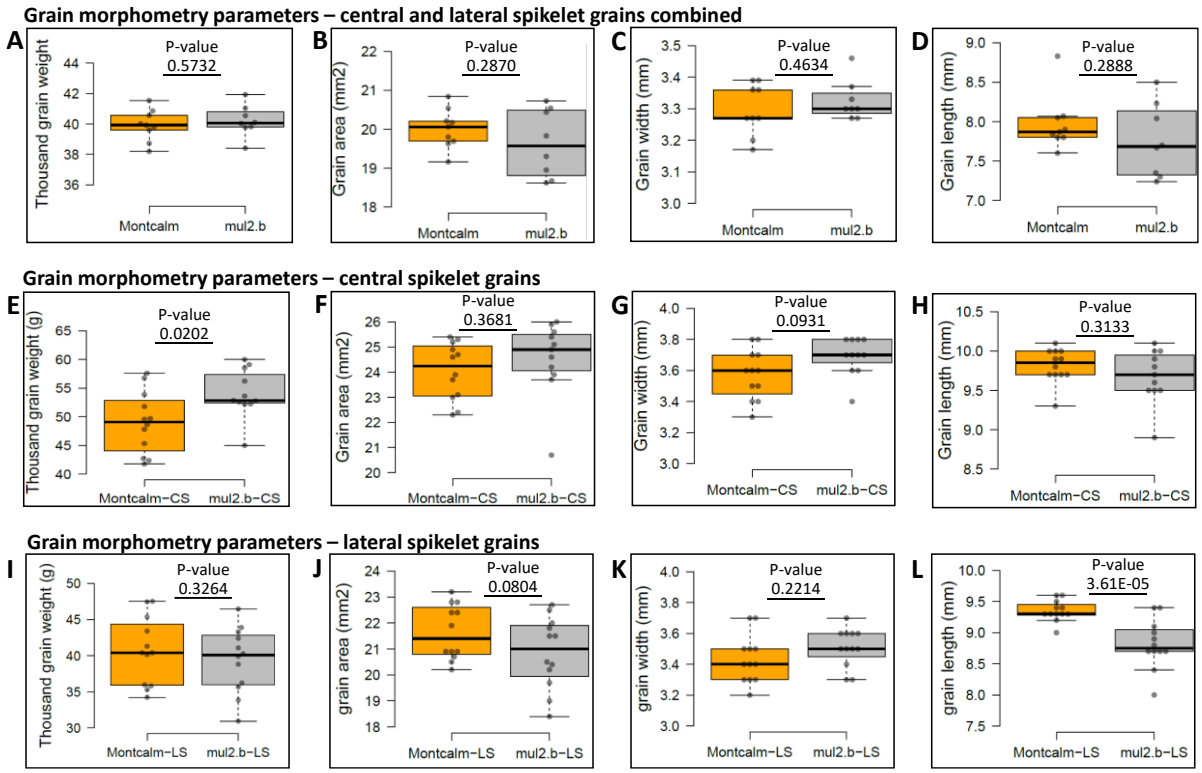

Supplementary figure 2. Grain morphometry parameters – Montcalm vs. *mul2.b*. (A-D) Thousand-grain weight (A), grain area (B), width (C), and length (D) of Montcalm and *mul2.b* measured from central and lateral spikelet grains together. (E-H) Thousand-grain weight (E), grain area (F), width (G), and length (H) of Montcalm and *mul2.b* measured from central spikelet grains. (I-L) Thousand-grain weight (I), grain area (J), width (K), and length (L) of Montcalm and *mul2.b* measured from lateral spikelet grains. P-values were calculated based on *Student's t-test* (two-tailed).

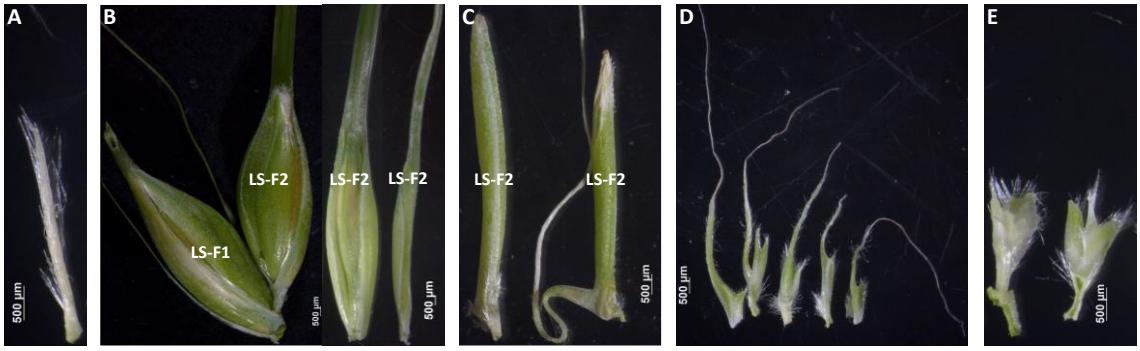

Wt – lateral spikelet rachilla | *mul2.b* – Class I phenotype | *mul2.b* – Class II | *mul2.b* – Class III | *mul2.b* – Class IV

Supplementary figure 3. *mul2.b* phenotype classification for lateral spikelet indeterminacy.

(A) Wild-type rachilla of Montcalm. (B-C) class I (B) and class II (C) additional florets excised from the lateral spikelets of *mul2.b*. (D-E) Malformed rachillae Class III (D) and class IV (E) rachillae excised from lateral spikelets.

	Spike 1			Spike 2			Spike 3			Spike 4			Spike 5			Spike 6			Spike 7			Spike 8			Spike 9			Spike 10			Spike 11			Spike 12		
	LL	CS	RL	LL	CS	RL	LL	CS	RL	LL	CS	RL	LL	CS	RL	LL	CS	RL	LL	CS	RL	LL	CS	RL	LL	CS	RL	LL	CS	RL	LL	CS	RL	LL	CS	RL
Node 37	!	!	!																																	
Node 36	!	!	!																						!	!	!	!	!	!						
Node 35	!	!	!																						!	!	!	!	!	!						
Node 34	!	!	!													!	!	!	!	!	!	!	!	!	!	!	!	!	!	!	!	!	!	!	!	!
Node 33	!	!	!	!	!	!	!	!	!	!	!	!				!	!	!	!	!	!	!	!	!	!	!	!	!	!	!	!	!	!	!	!	!
Node 32	!	!	!	!	!	!	!	!	!	!	!	!	!	!	!	!	!	!	!	!	!	!	!	!	!	!	!	!	!	!	!	!	!	!	!	!
Node 31	!	!	!	!	!	!	!	!	!	!	!	!	!	!	!	!	!	!	!	!	!	!	!	!	!	!	!	!	!	!	!	!	!	!	!	!
Node 30	!	!	!	!	!	!	!	!	!	!	!	!	!	!	!	!	!	!	!	!	!	!	!	!	!	!	!	!	!	!	!	!	!	!	!	!
Node 29	!	!	!	!	!	!	!	!	!	!	!	!	!	!	!	!	!	!	!	!	!	!	!	!	!	!	!	!	!	!	!	!	!	!	!	!
Node 28	!	!	!	!	!	!	!	!	!	!	!	!	!	!	!	!	!	!	!	!	!	!	!	!	!	!	!	!	!	!	!	!	!	!	!	!
Node 27	!	!	!	!	!	!	!	!	!	!	!	!	!	!	!	!	!	!	!	!	!	!	!	!	!	!	!	!	!	!	!	!	!	!	!	!
Node 26	!	!	!	!	!	!	!	!	!	!	!	!	!	!	!	!	!	!	!	!	!	!	!	!	!	!	!	!	!	!	!	!	!	!	!	!
Node 25	-	-	II	!	!	!	!	!	!	!	!	!	!	!	!	!	!	!	!	!	!	!	!	!	!	!	!	!	!	!	!	!	!	!	!	!
Node 24	-	-	-	!	!	!	!	!	!	!	!	!	!	!	!	!	!	!	!	!	!	!	!	!	-	-	-	-	-	-	!	!	!	!	!	!
Node 23	-	-	-	!	!	!	!	!	!	!	!	!	!	!	!	!	!	!	!	!	!	!	!	!	-	-	-	-	-	-	!	!	!	-	-	-
Node 22	-	-	II	-	-	-	!	!	!	!	!	!	!	!	!	!	!	!	!	!	!	-	-	-	-	-	-	-	-	-	!	!	!	-	-	-
Node 21	-	-	-	-	-	-	-	-	-	!	!	!	!	!	!	-	-	-	-	-	-	-	-	-	-	-	-	-	-	IV	-	-	-	-	-	-
Node 20	-	-	-	II	-	-	IV	-	IV	-	-	-	IV	-	-	-	-	IV	-	-	-	-	-	-	-	-	-	-	-	-	-	-	-	-	-	-
Node 19	-	-	-	-	-	-	-	-	-	-	-	-	-	-	-	-	-	-	-	-	IV	IV	-	-	-	-	-	-	-	-	-	-	-	-	-	-
Node 18	-	-	-	-	-	-	-	-	-	-	-	-	IV	-	IV	-	-	-	-	SS	-	-	-	-	-	-	-	I	-	I	-	-	-	-	-	-
Node 17	-	-	-	-	-	-	-	-	-	-	-	-	I	-	II	-	-	-	-	-	IV	-	-	-	IV	-	III	I	-	-	I	-	I	-	-	-
Node 16	-	SS	-	-	-	-	IV	-	-	-	-	-	-	-	-	-	-	-	-	-	-	I	-	IV	IV	-	-	I	-	I	IV	-	-	-	-	-
Node 15	-	SS	-	-	-	-	-	-	-	-	-	-	III	-	IV	-	-	-	-	-	IV	IV	-	-	IV	-	III	-	-	-	II	-	-	-	-	-
Node 14	-	-	-	-	-	-	-	-	-	-	-	-	III	-	IV	-	-	III	-	-	-	III	SS	-	-	-	III	-	-	I	-	-	IV	-	-	-
Node 13	-	SS	III	-	-	-	-	-	-	-	-	-	III	-	III	-	SS	-	-	-	-	III	-	III	I	-	IV	III	-	I	-	-	-	-	-	-
Node 12	-	SS	-	-	SS	-	-	-	-	-	-	-	I	-	I	-	SS	I	-	-	I	III	-	III	-	-	III	I	-	I	-	SS	III	-	-	-
Node 11	I	SS	-	III	-	-	-	-	-	-	-	-	I	-	-	IV	-	-	-	-	IV	I	-	-	III	-	III	I	-	I	-	-	-	-	-	-
Node 10	I	-	IV	III	-	III	-	-	-	-	-	-	I	-	IV	-	-	-	IV	-	IV	III	-	III	IV	-	IV	I	-	I	-	-	-	-	-	-
Node 9	-	-	I	I	-	-	-	-	III	-	-	III	I	-	I	-	-	-	IV	-	IV	I	-	III	I	-	III	I	-	I	-	SS	-	-	-	II
Node 8	I	-	-	-	-	-	-	-	III	-	-	-	I	-	I	-	-	-	IV	-	-	I	-	I	I	-	I	I	-	I	IV	-	-	-	-	-
Node 7	-	-	IV	-	-	-	-	-	-	-	-	-	I	-	I	-	-	-	I	-	I	IV	-	-	I	-	I	I	-	I	I	-	I	-	-	-
Node 6	III	-	IV	-	-	-	-	-	-	-	-	-	-	-	I	-	-	-	I	-	I	-	-	-	-	-	-	-	-	III	I	-	I	-	-	-
Node 5	-	-	-	IV	-	I	I	-	-	-	-	-	-	-	-	-	-	-	I	-	I	-	-	-	-	-	-	-	-	-	I	-	II	-	-	II
Node 4	-	-	-	I	-	-	I	-	III	I	-	-	-	-	-	-	-	-	-	-	-	-	-	-	-	-	-	-	-	-	-	-	-	I	-	-
Node 3	-	-	-	-	-	-	-	-	-	-	-	-	-	-	-	I	-	I	-	-	-	I	-	I	-	-	-	-	-	I	I	-	I	-	-	-
Node 2	I	I	I	I	-	-	-	-	I	-	-	-	I	-	I	-	-	-	I	-	-	-	-	-	-	-	-	I	-	I	I	-	-	-	-	-
Node 1	-	-	-	-	-	-	-	-	-	-	-	-	I	-	I	-	-	-	I	-	I	I	-	I	-	-	I	-	-	-	-	-	-	-	-	-
Class I	4		2	3		1	2		1	1		0	9		7	1		2	5		5	6		3	4		3	10		12	6		4	1		0
Class II	0		1	1		0	0		0	0		0	0		1	0		0	0		0	0		0	0		0	0		0	1		1	0		2
Class III	1		1	2		1	0		3	0		1	3		1	0		1	0		0	4		4	1		6	1		1	0		1	0		0
Class IV	0		3	1		0	2		1	0		0	2		4	1		1	3		6	3		1	4		2	0		1	2		1	0		0
SS		5			1			0			0			0			2			1			1			0			0			2			0	

Supplementary figure 4. Distribution of different classes of lateral spikelet indeterminacy and supernumerary spikelet phenotypes in spikes of the *mul2.b* mutant.

The yellow-colored cells at spikelet node 1 and in the upper spikelet nodes indicate the aborted spikelets at the base and top of the spike, respectively after anthesis. Cells highlighted in green indicate the fertile spikelets that potentially bear a grain. The cells in orange indicate the unfilled spikelets (spikelets formed but did not grow further). Classes, I, II, III, and IV indicate respective phenotypes for rachilla indeterminacy or additional floret formation in lateral spikelets, whereas SS is supernumerary spikelet phenotype in central spikelets. The notation "!" in the upper aborted spikelets indicates the absence of phenotypic information for lateral spikelet indeterminacy/additional spikelet and supernumerary spikelet phenotypes. CS – Central Spikelet; LL – Left Lateral spikelet; RL – Right Lateral spikelet; SS – Supernumerary spikelet.

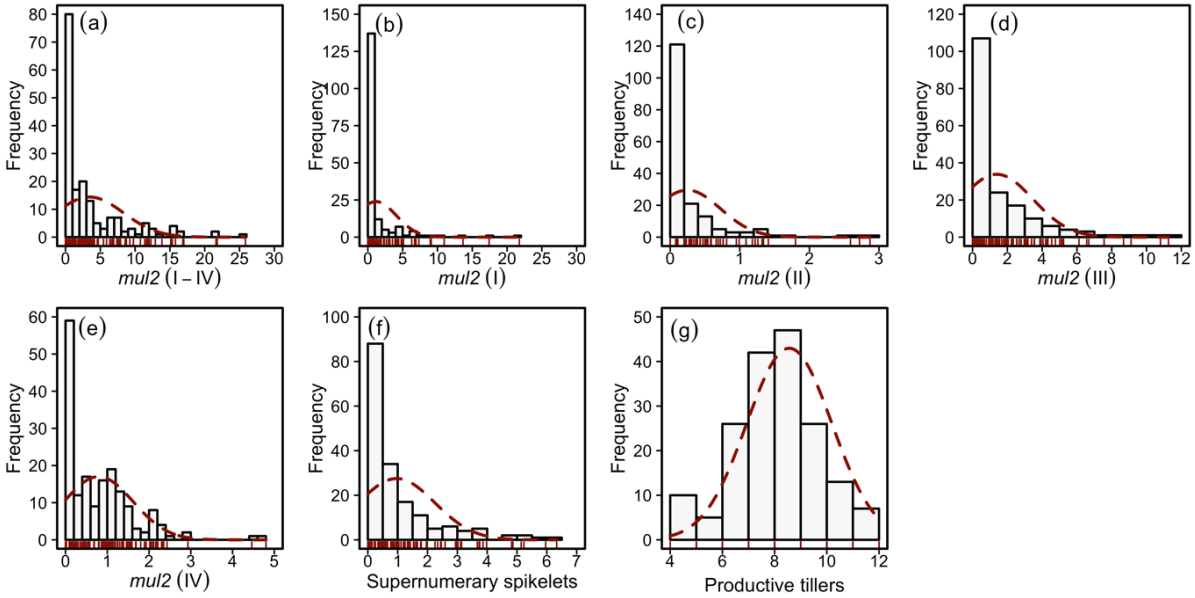

Supplementary figure 5. Frequency distribution of LS-IN and CS-SS phenotypes in Morex × *mul2.b* (POP 2016)

A

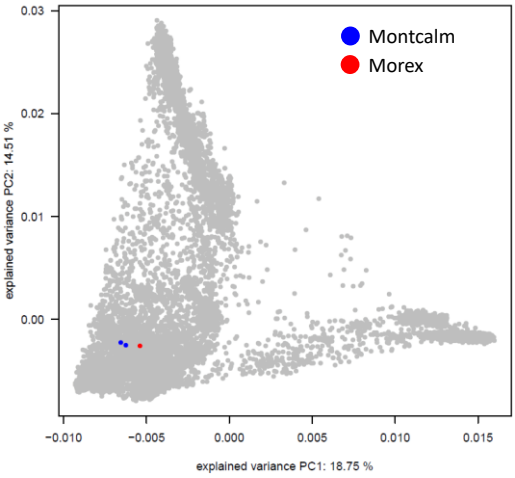

B

Chromosome	Markers/linkge group*	Linkage group length	Average inter-marker distance
1H	82	111.89	1.36
2H	101	188.66	1.87
3H(1)	12	18.15	1.51
3H(2)	24	27.75	1.16
3H(3)	56	59.10	1.06
4H	57	96.65	1.70
5H(1)	59	105.42	1.79
5H(2)	30	66.34	2.21
6H	93	114.43	1.23
7H(1)	79	104.13	1.32
7H(2)	12	23.46	1.96
Total/average	605.00	915.98	1.51

* Number of markers after filtration for <10% missing data/marker or filtration for two or more linked markers showing no recombination

Supplementary figure 6. Linkage map features – Morex × *mul2.b* (POP 2016)
(A) PCA plot of barley BRIDGE panel genotypes showing the high similarity between Montcalm (progenitor of *mul2.b* mutant) and Morex genotypes. (A) Features of genetic linkage maps for Morex × *mul2.b* – F_2 lines constructed using markers derived from genotyping by sequencing.

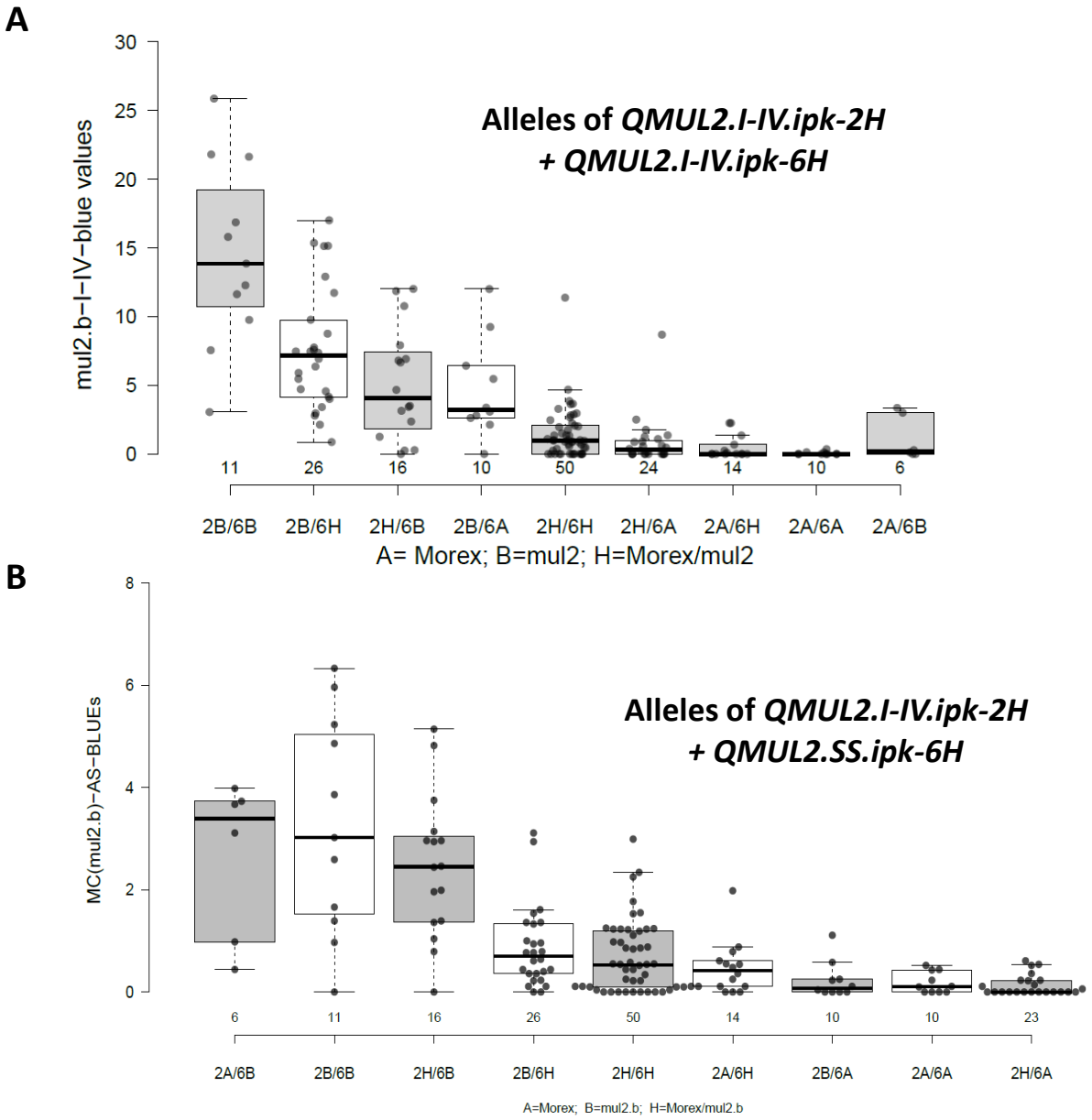

Supplementary figure 7. Phenotypic effect of LS-IN and CS-SS QTLs in Morex × *mul2.b*-F$_2$.

(A) Cumulative phenotypic effect of *QMUL2.I-IV.ipk-2H* and *QMUL2.I-IV.ipk-2H* QTL alleles (B) Cumulative phenotypic effect *QMUL2.I-IV.ipk-2H* and *QMUL2.SS.ipk-6H* QTL alleles. Phenotype frequencies shown in the box plots are derived from the genotypes of markers with the highest –log10 (p-value) and respective trait phenotype values.

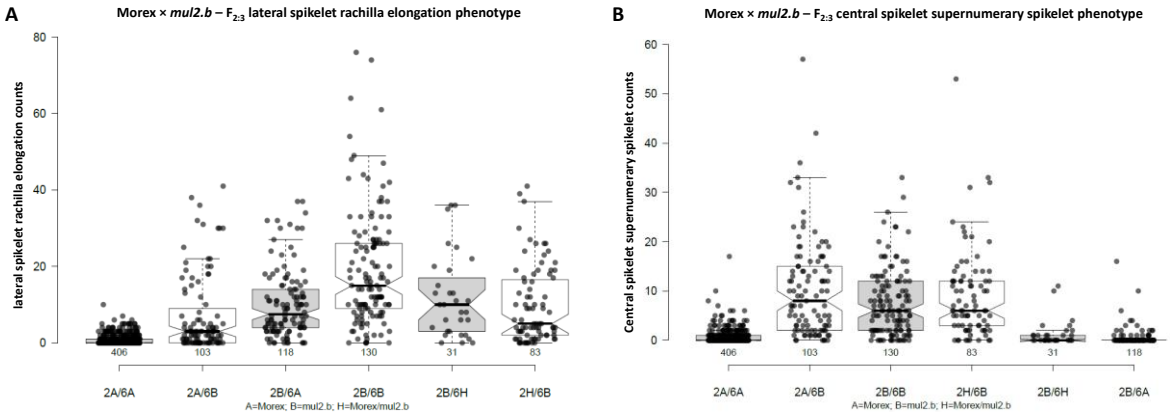

Supplementary figure 8. Phenotypic effect of LS-IN (A) and CS-SS traits (B) in $F_{2:3}$ progenies of Morex × *mul2.b*. The markers explaining the highest phenotypic value for the respective traits at 2H and 6H QTL were considered for the analysis.

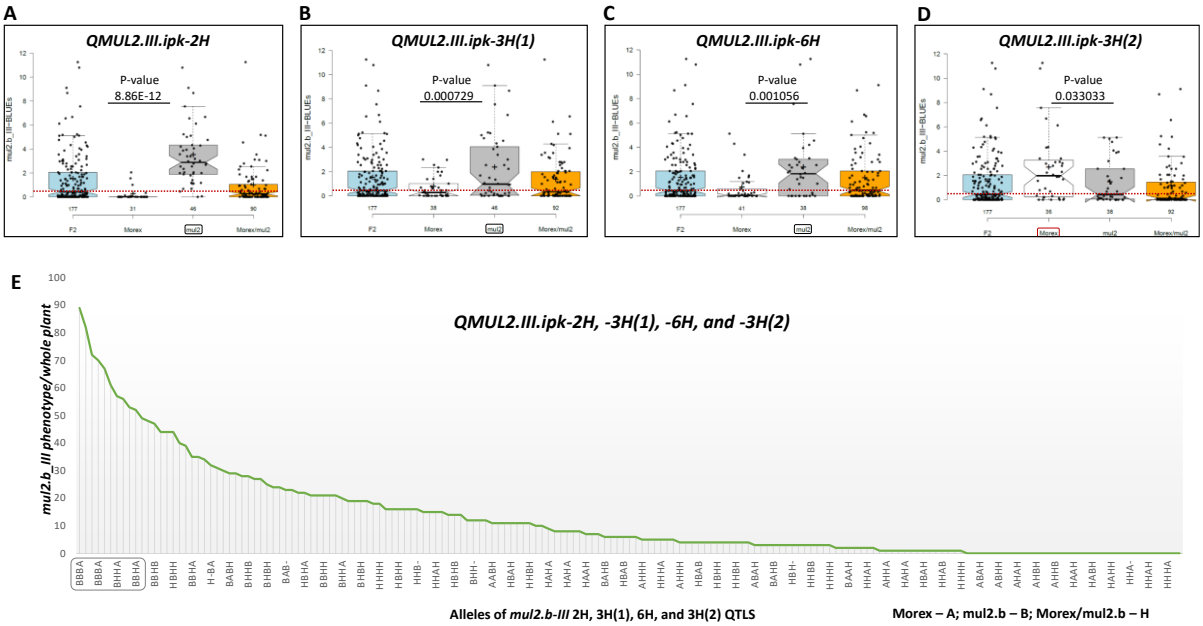

Supplementary figure 9. Phenotypic effect of LS-IN trait at individual QTLs *QMUL2.III.ipk-2H* (A) *QMUL2.III.ipk-3H(1)* (B) *QMUL2.III.ipk-6H* (C) and *QMUL2.III.ipk-3H(2)* (D). (E) The cumulative phenotypic effect from the four QTLs for class III LS-IN phenotype. Phenotype frequencies shown in the box plots are derived from the genotypes of markers with the highest –log10 (p-value) and respective trait phenotype values.

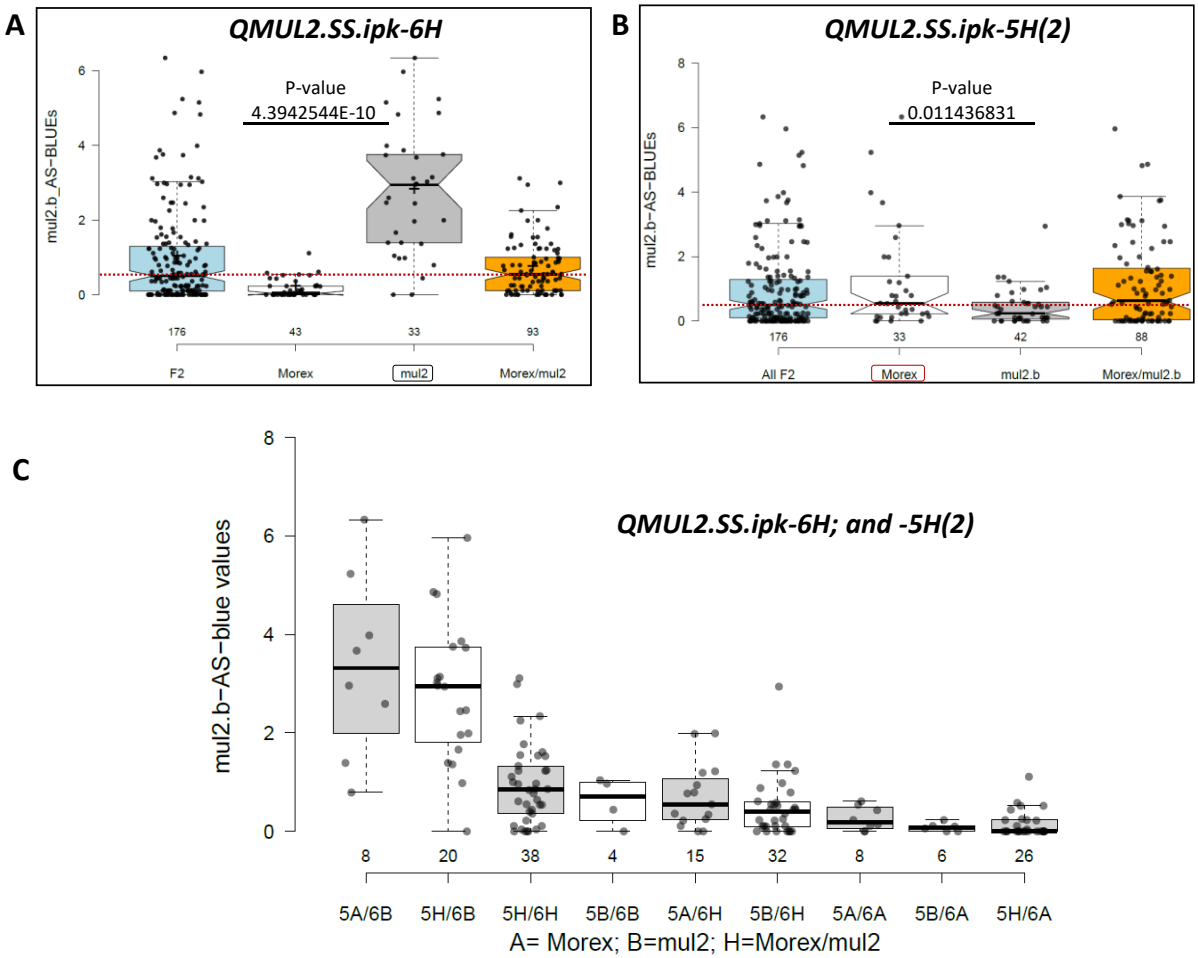

Supplementary figure 10. Phenotypic effect of CS-SS trait at individual QTLs *QMUL2.SS.ipk-6H* (A) and *QMUL2.SS.ipk-5H(2)* (B). (C)The cumulative phenotypic effect from both QTLs. Phenotype frequencies shown in the box plots are derived from the genotypes of markers with the highest –log10 (p-value) and respective trait phenotype values.

BM-NIL(*mul2.b*) *mul2.b* in Montcalm

Supplementary figure 11. CS-SS phenotype in BM-NIL(*mul2.b*) and *mul2.b* in Montcalm background.